Received: 23 August 2021 | Revised: 2 May 2022 | Accepted: 12 May 2022

DOI: 10.1002/met.2074

Meteorological Applications
Science and Technology for Weather and Climate
Open Access
RMetS

RESEARCH ARTICLE

Predictive skill of North American Multi-Model Ensemble seasonal forecasts for the climate rainfall over Central Africa

Armand Feudjio Tchinda[1,2] | **Roméo Stève Tanessong**[2,3] | **Ossénatou Mamadou**[1,4] | **Vanessa Tchida Diffo**[5] | **Zephirin Djomou Yepdo**[2,6] | **Jean Bio Chabi Orou**[1,7]

[1]Institut de Mathématiques et de Sciences Physiques (IMSP), Université d'Abomey Calavi (UAC), Porto-Novo, Benin

[2]Laboratory for Environmental Modeling and Atmospheric Physics (LEMAP), Department of Physics, Faculty of Science, University of Yaounde 1, Yaounde, Cameroon

[3]School of Wood, Water and Natural Resources, Faculty of Agronomy and Agricultural Sciences, University of Dschang-Cameroon, Ebolowa, Cameroon

[4]Laboratoire de Physique du Rayonnement (LPR), Faculté des Sciences et Techniques, Université d'Abomey Calavi, Godomey, Benin

[5]Chaire Internationale en Physique Mathématiques et Application (CIPMA-Chaire UNESCO), Laboratoire de la physique des matières Condensées, Université d'Abomey Calavi, Godomey, Benin

[6]National Institute of Cartography, Climate Change Research Laboratory (CCRL), Yaounde, Cameroon

[7]Laboratoire de Mécaniques des Fluides, de la Dynamique Non-linéaire et de la Modélisation des Systèmes Biologiques (LMFDNMSB), Porto-Novo, Benin

Correspondence
Armand Feudjio Tchinda, Institut de Mathématiques et de Sciences Physiques (IMSP), Université d'Abomey Calavi (UAC), Avakpa, BP: 613 Porto-Novo, Benin.
Email: armand.tchinda@imsp-uac.org and atchindafeudjio@yahoo.fr

Funding information
Region Scholarship Programme-IMSP Benin, Grant/Award Number: 57506853

Abstract

This study evaluates the predictive performance of the North American Multi-model Ensemble (NMME) over Central Africa (CA) using the historical rainfall data. The African Rainfall Climatology Version 2 (ARC2) is used as a substitute for reference observational data to examine the capability of 11 NMME and their NMME ensemble mean (MME) in simulating rainfall. Using the Kling-Gupta efficiency (KGE), Taylor skill score (TSS), and Heidke skill score, the predictive evaluation of the models is performed from lead 0 to lead 5 of each season. The results show that the NMME models satisfactorily reproduce the bimodal and unimodal structure of rainfall in CA at the lead 0 level of different seasons: December–February (DJF), March–May (MAM), June–August (JJA), and September–November (SON). The pattern correlation coefficient (PCC) shows values of NMME and MME greater than ∼0.69 and TSS > 0.60 for all four seasons. The MME presents a maximum in DJF 0.$\tilde{9}$6 between 0 and 1 month lead time. With the same time scale, just over 85% of the NMME have a KGE between 0 and 0.42. It follows that as the forecast lead time increases, the PCC and TSS of each model become small, with PCC 0.$\tilde{1}$2 in JJA and DJF,

TSS < 0.21 in JJA at lead 5. The NMME models exhibit an important rainfall bias and the calculated scores show the quality of the forecast decreases with increasing lead time; this may justify a constraint on the models to keep the good quality of the long-term seasonal forecast in CA.

KEYWORDS
lead time, NMME, rainfall, seasonal forecast, skill, Taylor skill score

1 | INTRODUCTION

Rainfall is a major component influencing the hydrological cycle over Central Africa (CA) (Sylla et al., 2010) and is important for agriculture and water resources. The improvement of forecasting for these water resources in CA countries is crucial nowadays, as their economies depend on it (Biman et al., 2004). In addition, agriculture in CA is mainly rain-fed and sensitive to climate fluctuations (Clover, 2003), which can affect income sources, food security, and national economic development (Fotso-Nguemo et al., 2017; Tanessong et al., 2020). Due to the importance of seasonal and interannual meteorological variability in the region, useful long-lead forecasts of meteorological conditions (Ogallo & Oludhe, 2009) are necessary to provide guidance for timely action (Hillbrumer & Moloney, 2012) to mitigate potential humanitarian disasters.

Global climate models (GCMs) have been upgraded in recent years through scientific advances and the incorporation of global data (Bauer et al., 2015; Molteni et al., 2011). Today major climate centres worldwide use GCMs to generate operational climate forecasts up to ~11 months into the coming year (Demargne et al., 2014; Donner et al., 2011). For example, the National Centers of Environmental Prediction (NCEP) of the United States uses the Climate Forecast System version 2 (CFSv2) (Saha et al., 2014), the Canadian Meteorological Centre (CMC) uses the coupled Climate Model versions 3 and 4 (CanCM3 and CanCM4; Merryfield et al., 2013). The North American Multi-Model Ensemble (NMME) (Kirtman et al., 2014) system incorporates seasonal forecasts of different hydro-climatic variables from several American and Canadian climate centres.

These forecasts are invaluable for many scientific and operational applications, especially precipitation forecasting (Cash et al., 2019; Krakauer, 2019; Setiawan et al., 2017), forecasting extremes (Yuan et al., 2015), atmospheric rivers (Zhou & Kim, 2018), drought (Hao et al., 2017; Yao & Yuan, 2018). As in any other multimodel environment, the NMME models show mixed predictive skills in terms of seasonal and sub-seasonal predictions. Many previous studies have already been carried out to assess the skills of NMME models around the world. H. Wang (2014) assessed seven NMME models for the Continental United States and found that the uncertainty of rainfall forecast is greater in the western United States in summer. Thober et al. (2015) investigated NMME in the context of drought forecasting in Europe and observed that the soil moisture has variability in space and time of up to 40%. Slater et al. (2019) evaluated the precipitation and temperature forecasting of eight NMME models in relation to their relative climatology over seven large regions of the United States and found that the models perform better in predicting droughts than floods on a seasonal scale. These authors observed that skill deteriorates rapidly with increasing lead time. Setiawan et al. (2017) investigated the precipitation hindcasts from seven NMME models over South Sulawesi and found that the hindcasts were more skillful during June–November and weakest during December–May. By using a principal component analysis on the anomaly correlations of 10 sets of global rainfall forecasts from the NMME models, Zhao et al. (2018) found that their skills depend on the accuracy of the data assimilation algorithm. Recently, Singh et al. (2019) investigated the performance of seasonal mean and interannual variability representation of Indian summer monsoon rainfall using nine global coupled ocean–atmosphere models participating in phase 1 (NMME 1) and nine global coupled ocean–atmosphere models participating in phase 2 (NMME 2). They found that the NMME models represent Indian monsoon rainfall with modest skill and systematic biases. Roy et al. (2020) assessed 16 NMME models using the Kling-Gupta efficiency (KGE) for precipitation and temperature variables. Then, using an empirical orthogonal function, they examined the spatiotemporal variability structures of the forecasts. These results showed that rainfall skill was highest during the first lead time and decreased rapidly thereafter. Overall, these authors noted that the rainfall skill of models was the largest for the CMC, National Aeronautics and Space Administration (NASA), Geophysical Fluid Dynamics Laboratory (GFDL), and NCEP models (see Table 1).

TABLE 1 Eleven North American Multi-Model Ensemble forecasts studied in this paper

Models	Organization	Ensemble size	Lead time (month)
CanCM3	CMC	10	0–11
CanCM4	CMC	10	0–11
CCSM3	COLA-RSMAS	6	0–11
CCSM4	COLA-RSMAS	10	0–11
FLOR-AO6	GFDL	12	0–11
FLOR-BO1	GFDL	12	0–11
CFSV1	NCEP	15	0–8
CFSV2	NCEP	24	0–9
CESM1	NCAR	10	0–8
GEN-NEMO	GFDL	10	0–11
IRI-CHAMP5	GFDL	12	0–7

Abbreviations: CMC, Canadian Meteorological Centre; COLA-RSMAS, Center for Ocean-Land-Atmosphere Studies-Rosenstiel School of Marine and Atmospheric Science; GFDL, Geophysical Fluid Dynamics Laboratory; NCAR, National Center for Atmospheric Research; NCEP, National Centers for Environmental Prediction.

In Africa, Shukla et al. (2016) were the first who assessed eight NMME forecasts over East Africa (EA). Their results revealed that the models perform better over a small portion of the domain. In addition, they noted that NMME models were incompetent in simulating interannual variability, but that rainfall prediction was stronger during El Niño Southern Oscillation (ENSO) years. Shukla et al. (2016) also showed that NMME ensemble mean (MME) performance is as good as that of individual models. In the Sahelian region, Giannini et al. (2020) evaluated the deterministic skill of the NMME models and found that the models predicted July–September Sahel-wide rainfall as skillfully in February–March as in June. The predictability of Ethiopian Kiremt rainfall (June–September: JJAS) and forecast skill of the European Centre for Medium-Range Weather Forecasts fifth-generation seasonal forecast system 5 were explored during 1981–2019 by Ehsan et al. (2021). The authors showed that the ENSO is the main modulator of the Kiremt rainfall variability. In Ethiopia, Acharya et al. (2021) in their studies used the next generation (NextGen) system based on a calibrated multi-model ensemble approach that utilizes Global Climate Models (GCMs) from the NMME project. Their studies were conducted over three seasons, namely Belg: February–May, Kiremt: June–September, and Bega: October–January. After calibrating the GCMs predictions with the observations, they found that the resulting predictions are characterized by moderate skill at lead 1. In addition, they found that the NextGen forecasting system shows the highest deterministic and probabilistic skills in rainfall areas of Bega compared with Kiremt and Belg. Recently, Teshome et al. (2022) evaluated the predictive skill of NMME models from JJAS using canonical correlation analysis and root mean square error. Their results indicate that the models were able to capture rainfall during JJAS over central, northern, and northeastern Ethiopia while showing poor or limited skill over western and southwestern Ethiopia. In CA, Tchinda et al. (2022) recently assessed the skill of NMME models over the four seasons: December–February (DJF), March–May (MAM), June–August (JJA), and September–November (SON) using categorical and deterministic methods. They found that between 0 and 2 months lead time, the MME well reproduces the rainfall peak of the Atlantic coast and in the East of Democratic Republic of Congo in MAM and SON. In addition, the MME using categorical scores shows that the probability of detection and critical success index for normal seasons are high and remain very low for above and below-normal seasons.

Despite an increasing number of analyses focused on assessing the skill of NMME models, CA has received little attention in the field of seasonal forecasting compared with EA and South Africa. In addition, minor information is known about the skill of NMME to predict different seasons in CA. Although the recent study done by Tchinda et al. (2022) provided background and some important aspects of NMME models in this region, a systematic evaluation of different models and seasons is still lacking, thus many perspectives remain unexplored.

The previous work done by Tchinda et al. (2022) in CA using NMME models has some shortcomings, namely, the authors limited themselves to the MME without considering the predictive skill and climatology of each individual NMME model, while the NMME models' outputs are produced independently (see Table 1). Model developers may need information about each individual model to better

improve their models. In addition, the hypothesis that the predictive skill of some individual models may approach the MME was not verified. Also, they did not evaluate the skill of NMME models for the SST indices Niño3.4 (5° S–5° N, 170°–120° W), SST anomalies over the western pole (IODWP, 10° S–10° N, 50°–70° E), and eastern pole (IODEP, 10° S–0°, 90°–110° E). Nevertheless, the teleconnection ENSO and Indian Ocean Dipole (IOD) is the main source of seasonal forecast predictability.

Thus, to address the above gaps, the research questions we investigate in this study are (1) on a seasonal scale, what is the predictive skill of the 11 NMME models in CA? (2) Do NMME models succeed in reproducing the climatology in CA? (3) In this region are some models more similar to the multi-model ensemble (MME)? (4) What are the skills of NMME models to simulate SST indices Niño3.4, IODWP, and IODEP?

These issues have major applications for seasonal, hydrological, and meteorological forecasts in CA and must be addressed. In addition, this study will be useful in this region where agriculture is mainly rain-fed and extremely sensitive to climate fluctuations.

The objective of this paper is to assess the performance of the 11 NMME models over four seasons; DJF, MAM, JJA, and SON at different lead times, which is beneficial for (1) model developers to improve their models (2) users of seasonal forecasts to know which models to use in CA. Section 2 presents the details of the models and African Rainfall Climatology Version 2 (ARC2) observations employed in the analysis. The assessment of the models performance and discussions of the results are presented in Section 3. Finally, Section 4 presents the summary and conclusion of this study.

2 | DATA AND METHODS

2.1 | Data

The assessment skill is carried out using 11 NMME forecasts; see Table 1 (Kirtman et al., 2014). The number of ensembles in each of these models ranges from 6 to 24. The term lead time of each NMME indicates the period between the forecast's initialization time and the predicted month. For example, in the case of the MAM, forecasts initialized in March are called lead 0, and forecasts initialized on October 1 (of the previous years) are called lead 5 as in Shukla et al. (2016). The seasonal forecast initialized in March is calculated as the sum of the March forecast at lead 0.5, April forecast at lead 1.5, and May forecast at lead 2.5. MAM lead 1 is calculated as the sum of the March forecast at lead 1.5, April forecast at lead 2.5, and May forecast at lead 3.5, as in Slater et al. (2019). Two of these models are Canadian and the others are from various organizations in the United States, such as the NASA, National Oceanic and Atmospheric Administration (NOAA), National Center for Atmospheric Research (NCAR), NCEP, and Columbia University. The NMME data have been downloaded from https://iridl.ldeo.columbia.edu/ on a grid resolution 1° × 1°. The hindcast is used for a common period of 27 years (1983–2009). In this study, ARC2 (Novella & Thiaw, 2013) is used as the reference data source. The resolution grid is 0.1° × 0.1°. This resolution grid has been remapped and cropped into the NMME grid using the conservative first-order remapping approach (Jones, 1999). The optimum interpolation version 2 (OI) analysis of Reynolds et al. (2002) is used in this study to evaluate the SST Niño3.4, IODWP, and IODEP indices. The native resolution of the Reynolds et al. (2002) SST is 1° × 1°. This analysis, produced at NOAA, uses both satellite data and in situ records from ships and buoys (E. Becker et al., 2014). CA's topography is shown in Figure 1 and is defined by the coordinates 5° E–33° E (longitude) and 15° S–16° N (latitude).

2.2 | Methodology

2.2.1 | Multi-model ensemble method

Firstly we construct the ensemble mean (EM) of each individual NMME. It is given by the equation below

$$Q_{\mathrm{ens}}(\mathrm{s,j,m,p}) = \sum\nolimits_n Q(\mathrm{s,j,m,n,p})/N, \qquad (1)$$

where the parameters s, j, m, n, p are the time (s), the longitude (j), the latitude (m), the ensemble members (n), and the lead time (p), respectively. The number of members ranges from $n = 1,\ldots, N$, where N is the total number of each member of the NMME forecast. In addition, the MME is formed by averaging together the EMs of all the Z models, as in E. Becker et al. (2014). The MME is given by the equation below.

$$Q_{\mathrm{NMME}}(\mathrm{s,j,m,p}) = \sum\nolimits_z Q_{\mathrm{ens},z}(\mathrm{s,j,m,p})/Z, \qquad (2)$$

where Z is the total number of NMME forecasts and ranges from $z = 1,\ldots, Z$. Thus, after constructing the EM and MME, the climatology of the 11 models over the study period (1983–2009) is calculated over the four seasons; DJF, MAM, JJA and SON and compared with the climatology of the ARC2 observations. The individual biases between the ARC2 and each model are computed as the difference between the observation and the

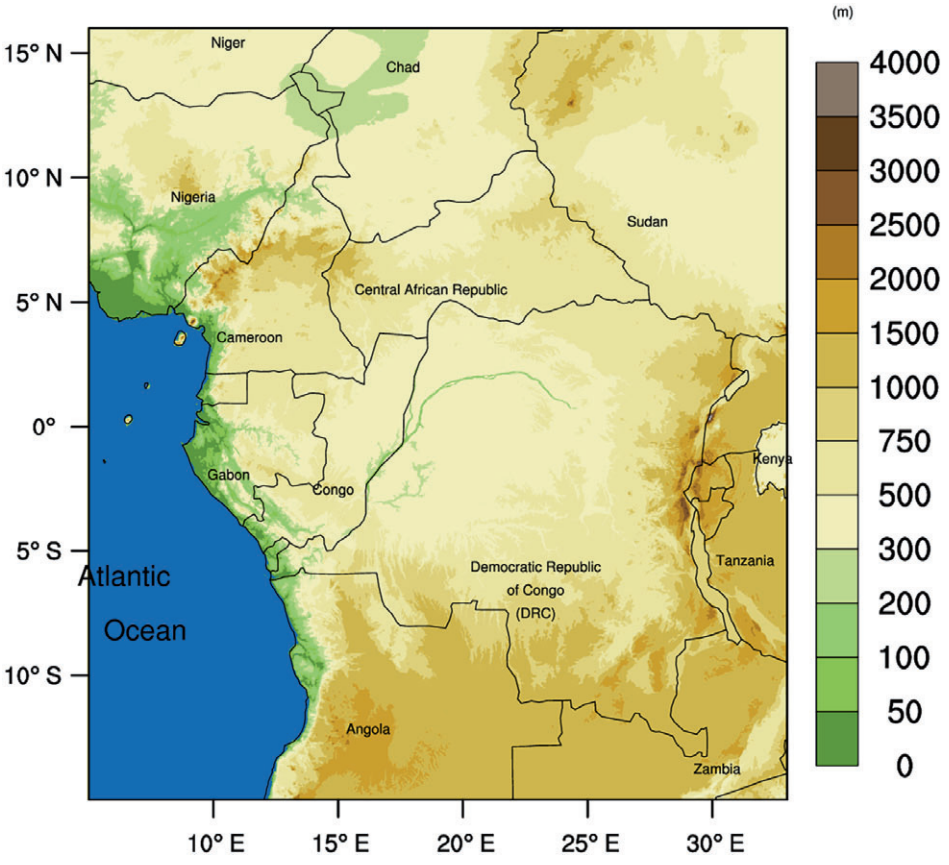

FIGURE 1 Central Africa (CA) topography of the study area located 5° to 33° longitude and −15° to 16° latitude.

forecast, allowing us to highlight which part of CA the model underestimates or overestimates.

2.2.2 | Forecasting skill and predictability

The performance of NMME models is assessed based on the Taylor diagram (TD) and Taylor skill score (TSS) (Taylor, 2001; B. Wang et al., 2018). These approaches are widely used to assess the degree of similarities and differences between the models and the observation. In this study, the TD summarizes the ratio of spatial SD and pattern correlation coefficient (PCC) between the ARC2 and each individual NMME of the 0–5 month lead time. The TSS (Babaousmail et al., 2021; Zhu et al., 2020) is calculated using the equation below.

$$\mathrm{TSS} = 4(1+\mathrm{PC})^2 / \left[\left(\frac{\sigma_{\mathrm{NMME}}}{\sigma_{\mathrm{OBS}}} + \frac{\sigma_{\mathrm{OBS}}}{\sigma_{\mathrm{NMME}}}\right)(1+\mathrm{PC_o})^2\right], \quad (3)$$

where PC is the spatial pattern correlation coefficient between the models outputs and the ARC2. The $\mathrm{PC_O}$ is the highest value of PC that can be reached (here, we set the threshold ∼0.99999). The variables σ_{OBS} and σ_{NMME} represent the SD of the ARC2 and NMME, respectively. The threshold value score of ∼1 shows a perfect match between the NMME models and the observation, whereas 0 expresses contrary models performance. The details on the techniques and applications of TSS can be found in Chen et al. (2011), Ngoma et al. (2021), and Zhu et al. (2020). In addition to these metrics, the skill of the forecasts was assessed using the KGE (Gupta et al., 2009; Kling et al., 2012; Roy et al., 2020).

KGE varies from $-\infty$ to 1 and is given by

$$\mathrm{KGE} = 1 - \sqrt{(r-1)^2 + (\eta-1)^2 + (\varphi-1)^2}. \quad (4)$$

The parameters η, φ, and r in Equation (4) represent the bias error, variability error, and correlation coefficient, respectively. They are given in Equations (5) and (6) below.

$$\eta = \frac{\mu_{\mathrm{nmme}}}{\mu_{\mathrm{observ}}}, \quad (5)$$

$$\varphi = \frac{\mathrm{COV_{nmme}}}{\mathrm{COV_{obser}}}, \quad (6)$$

where the parameters μ_{nmme}, μ_{obsev}, $\mathrm{COV_{nmme}}$, and $\mathrm{COV_{obsev}}$ represent the mean model, mean observation, coefficients of variation (ratio of SD to mean) of NMME, and

coefficients of variation of the observations,respectively. In the equation (4), r is the correlation coefficient between each individual models and the reference observation ARC2.

2.2.3 | Categorical skill MME

In this part, using a contingency table (see Table 2), the rainfall of each season is categorized into three classes: dry (D), normal (N), and rainy (R). With D for precipitation anomaly below -0.43σ, N for the precipitation anomaly between -0.43σ and 0.43σ, and R for precipitation anomaly above 0.43σ (Stankis et al., 1989; Tchinda et al., 2022; Tippett et al., 2007). The contingency table allows us to calculate the Heidke skill score (HSS) (Barnston, 1992) and the accuracy between the MME and the observation. The HSS is a skill score for categorical forecast where the correct proportion is rescaled with the reference point of correct forecasts due to random chance. The score varies from $-\infty$ to 1. The HSS is given by Equation (7) and the accuracy by Equation (8) below.

$$\mathrm{HSS} = \frac{(n_{11}+n_{22}+n_{33}) - \left(\frac{n_{.1}\,n_{1.}\,+n_{.2}\,n_{2.}\,+n_{.3}\,n_{3.}}{n_t}\right)}{n_t - \left(\frac{n_{.1}\,n_{1.}\,+n_{.2}\,n_{2.}\,+n_{.3}\,n_{3.}}{n_t}\right)}. \quad (7)$$

$$\mathrm{Accuracy} = \frac{1}{n_t}(n_{11}+n_{22}+n_{33}), \quad (8)$$

where the expressions of the parameters $n_{.1}$, $n_{.2}$, $n_{.3}$, $n_{1.}$, $n_{2.}$, and $n_{3.}$ in Equation (7) are given by Equations (9), (10), (11), (12), (13), and (14) respectively (see Table 2).

$$n_{.1} = n_{11}+n_{21}+n_{31}, \quad (9)$$

$$n_{.2} = n_{12}+n_{22}+n_{32}, \quad (10)$$

$$n_{.3} = n_{13}+n_{23}+n_{33}, \quad (11)$$

$$n_{1.} = n_{11}+n_{12}+n_{13}, \quad (12)$$

$$n_{2.} = n_{21}+n_{22}+n_{23}, \quad (13)$$

$$n_{3.} = n_{31}+n_{32}+n_{33}. \quad (14)$$

TABLE 2 Contingency table used to calculate Heidke skill score and accuracy

		Observations			
		D	**N**	**R**	**D+ N+ R**
Forecast	D	n_{11}	n_{12}	n_{13}	$n_{1.}$
	N	n_{21}	n_{22}	n_{23}	$n_{2.}$
	R	n_{31}	n_{32}	n_{33}	$n_{3.}$
D+ N+ R		$n_{.1}$	$n_{.2}$	$n_{.3}$	n_t

In Equations (8), (9), (10), (11), (12), (13), and (14), the parameters n_{11}, n_{22}, n_{33} represent the number of years correctly predicted dry, normal, and rainy respectively (see Table 2). The parameter n_{21} is the number of years predicted normal and observed dry, n_{31} is the number of years predicted rainy and observed dry, n_{12} is the number of years predicted dry and observed normal, n_{32} is the number of years predicted rainy and observed normal, n_{13} is the number of years predicted dry and observed rainy, n_{23} is the number of years predicted normal and observed rainy, n_t is the total number of years in the study period (1983–2009).

The HSS is a metric of the potential increase in the number of correct forecasts over random forecasts.

2.2.4 | Predictive skill of the SST indices Niño3.4, IODWP and IODEP

The performance of NMME models to simulate SST Niño3.4 (5° S–5° N, 170°–120° W), SST anomalies over the western pole (IODWP, 10° S–10° N, 50°–70° E), and eastern pole (IODEP, 10° S–0°, 90°–110° E) is evaluated using the ratio of SD and anomaly correlation coefficient (ACC) between the observation SST and each individual model (called as the skill of the model) as in Pillai et al. (2018). ACC is a measure of the association between predicted and observed anomalies. The EM anomalies of each individual NMME are constructed by averaging the individual members into the EM, subtracting the model's own 1983–2009 average climatology as in E. Becker et al. (2020). In this study, ACC and SD for each model were calculated from 0 to 5 months lead time over the four seasons DJF, MAM, JJA, and SON.

3 | RESULTS AND DISCUSSIONS

3.1 | Seasonal mean climatology rainfall

Figure 2 shows seasonal rainfall climatology over CA of the NMME models (see Table 1), MME at lead 0, and ARC2 observation for DJF, MAM, JJA, and SON. The spatial distributions of rainfall biases from the NMME and MME forecasts for the four seasons are shown in Figure 3 at lead 0. The seasonal distribution of rainfall over CA is largely affected by the movement of the Intertropical Convergence Zone (ITCZ), this is more visible on

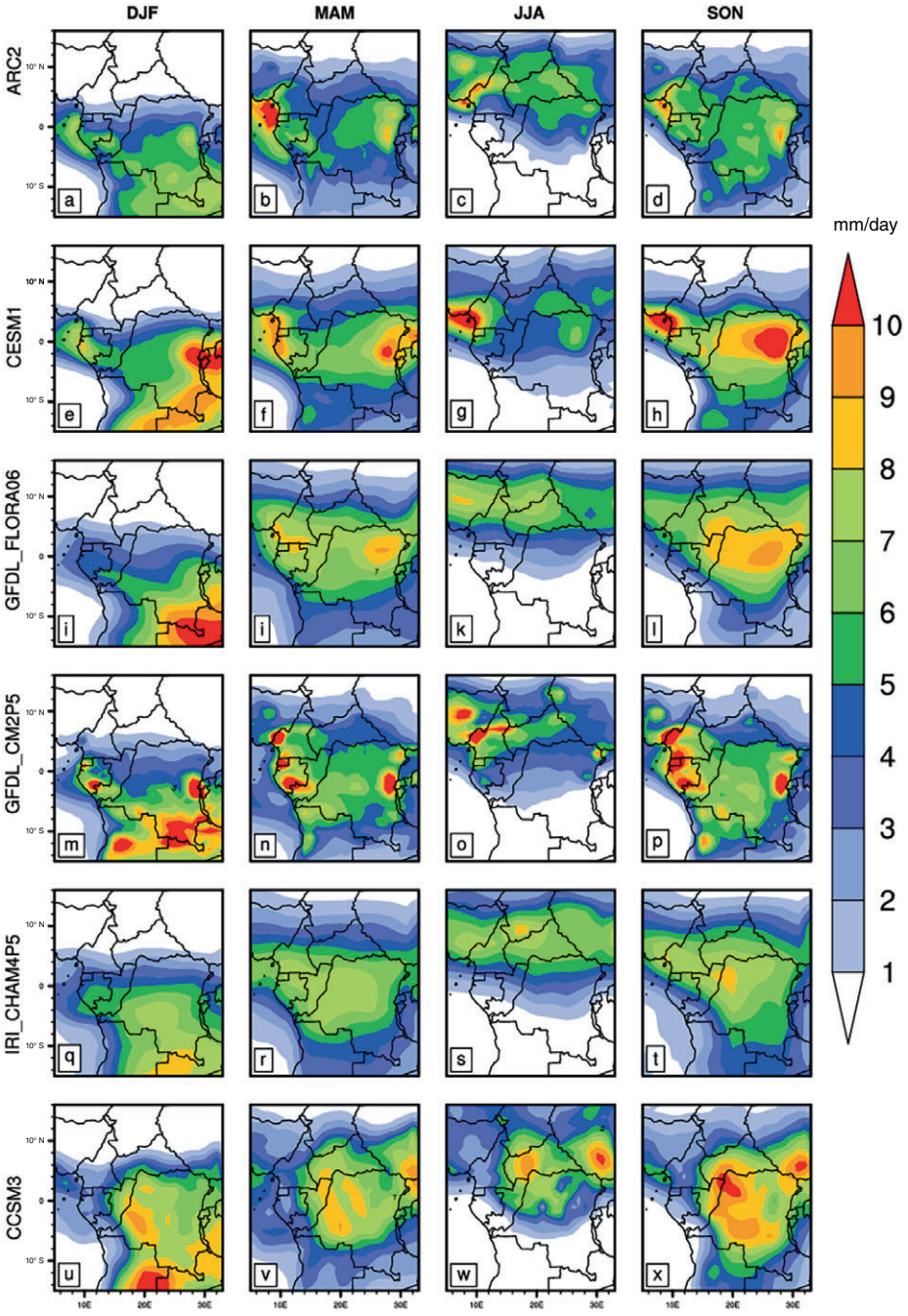

FIGURE 2 Climatology (1983–2009) rainfall (in millimetres per day) from North American Multi-Model Ensemble (NMME) and observation ARC2 of the four seasons. The first column represents the December–February (DJF), the second column the March–May (MAM), the third the June–August (JJA), and the fourth the September–November (SON). Rows 1, 2, 3, 4, 5, 6 represent the observation ARC2, and models CESM1, GFDL FLORAO6, GFDL CM2P5, IRI CHAM4P5, CCSM3 (see Table 1) at lead 0 respectively. Climatology (1983–2009) rainfall (in millimetres per day) NMME models of the four seasons at lead 0. The first column represents the DJF, the second column the MAM, the third the JJA, and the fourth the SON. Rows 1, 2, 3, 4, 5, 6, 7 represent the models CFSV2, CFSV1, CanCM3, CanCM4, GEN-NEMO, CCSM4, and ensemble (MME).

the observation ARC2 (see Figure 2). During the MAM, the Congo Basin (CB) locality is the most humid, with a large amount of rainfall near the Guinea coast, as shown by NCEP CFSV1, NCEP CFSV2, GFDL CM2P5, CESM1, CanCM3, and MME (see Figure 2d′,d″,h′,r,i′) because of vegetation and high convective activity. The maximum rainfall of ∼9 mm/day is most remarkable during this season in the NCEP CFSV1 model over most parts of southern Cameroon and all of Gabon. Also in MAM, the MME has a maximum rainfall of 7̃.5mm/day in the

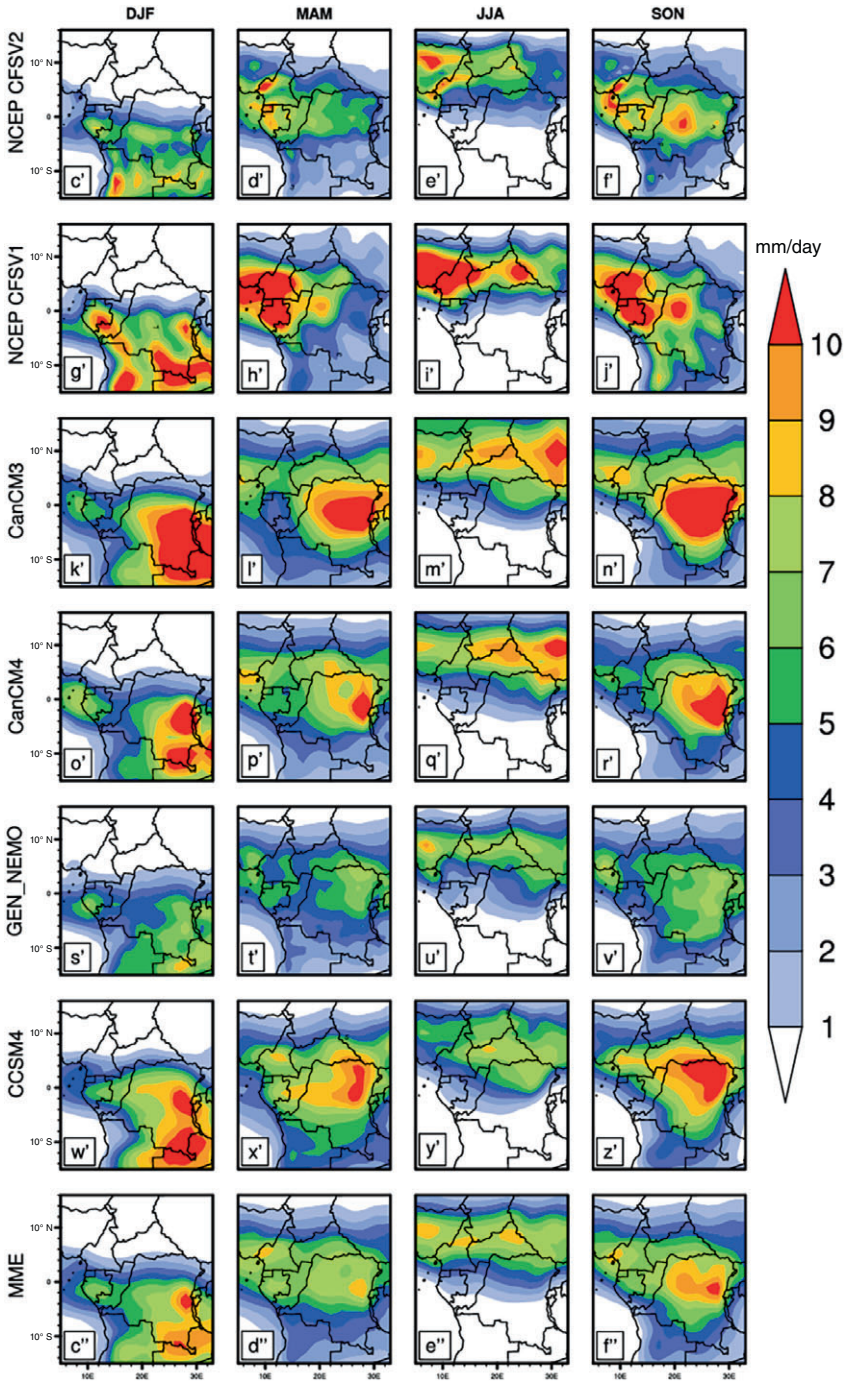

FIGURE 2 (Continued)

Eastern Democratic Republic of Congo. During the JJA, maximum rainfall is seen over the whole northern part of CA with high rainfall peaks around Mount Cameroon (southwestern Cameroon) for the NCEP CFSV1, NCEP CFSV2, CM2P5, CESM1 models (see Figure 2e′,j′,s,k). It is also noted that during this season, the MME shows rainfall peaks of $\tilde{8}$ mm/day over northern Cameroon and the Eastern Central African Republic compared to the CanCM4 and CanCM3 models which show rainfall maxima of ∼10 mm/day. Some previous studies have shown that the increase in rainfall over this area is caused by the transport of humidity from the ocean to the southwest (Pu & Cook, 2010). During SON, the highest precipitation from NMME models is observed over the Gulf of Guinea (see NCEP CFSV1), CB (see CCSM3 and CCSM4, CanCM3 and CanCM4, CESM1 and MME). Analysis of the DJF shows that the southern part of CA receives the highest rainfall, which is due to

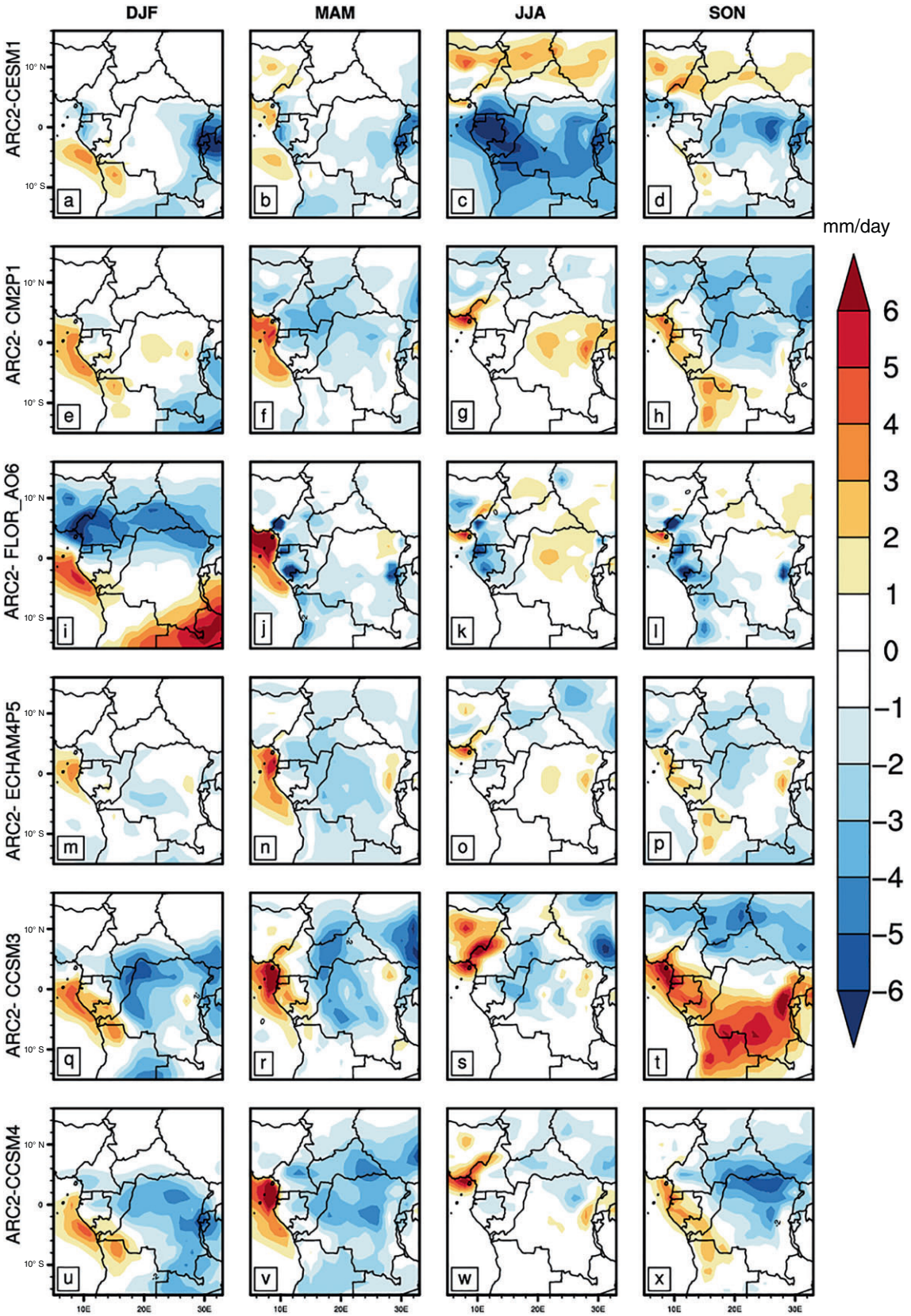

FIGURE 3 Bias (in millimetres per day) between ARC2 observation and North American Multi-Model Ensemble (NMME) forecast (CESM1, GFDL-FLOR AO6, IRI-CHAM4P5, and CCSM4). Columns 1, 2, 3, 4 represent the four seasons December–February (DJF), March–May (MAM), June–August (JJA), and September–November (SON), respectively. Bias (in millimetres per day) between ARC2 observation and NMME models (CFSV1, CFSV2, CanCM3, CanCM4, GEN-NEMO, MME). Columns 1, 2, 3, 4 represent the four seasons DJF, MAM, JJA, and SON, respectively.

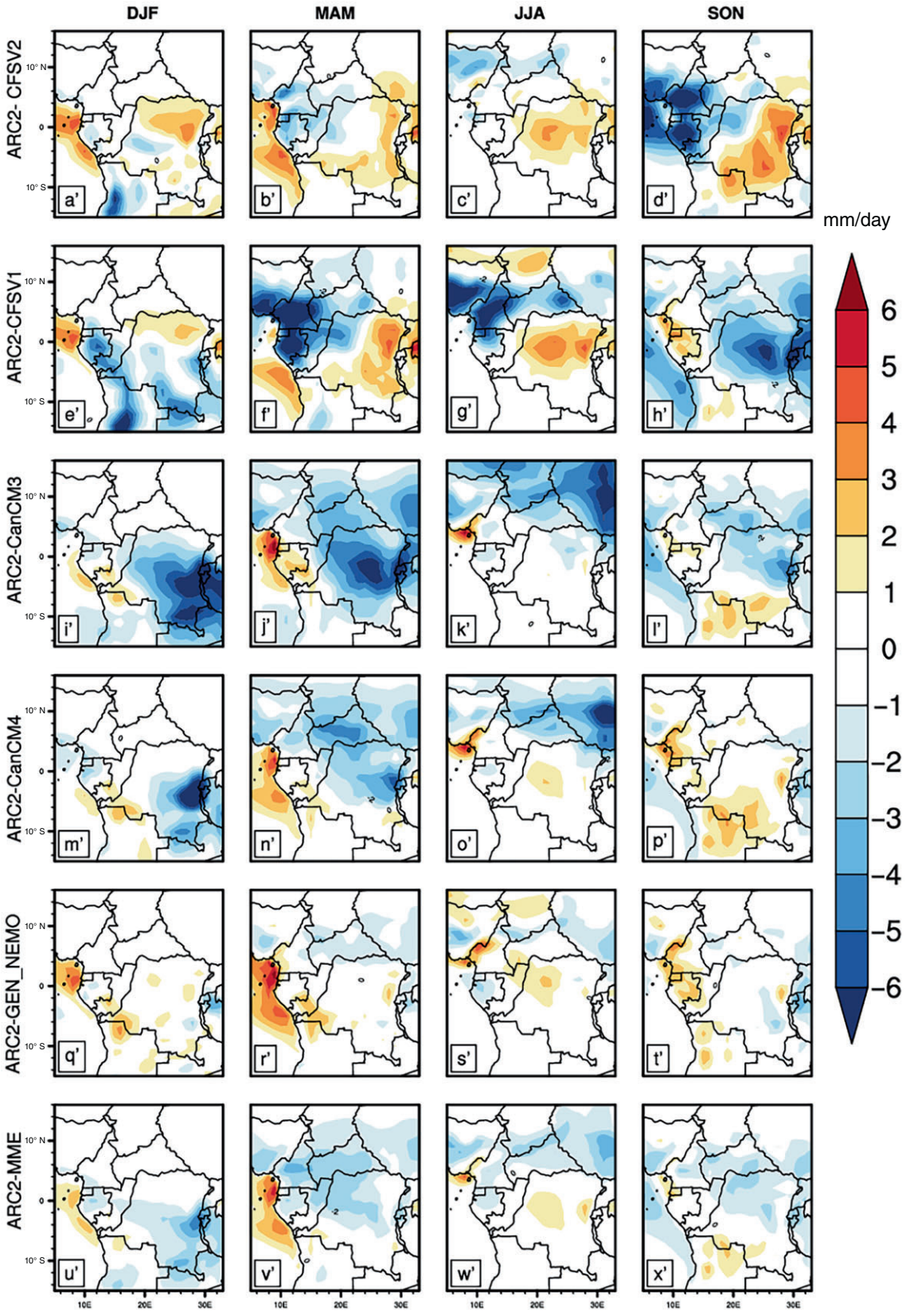

FIGURE 3 (Continued)

the presence of high humidity and higher summer sunshine that ameliorate the atmospheric convection, producing large rainfall in this part of the region (Simon et al., 2015; Tamoffo et al., 2019). There are other important mechanisms such as topography, African easterly jet, low-level jets, sea surface temperatures,

among others that result in the observed spatial distribution of rainfall (Aloysius et al., 2016; Nicholson & Dezfuli, 2013; Tierney et al., 2013; Washington et al., 2013) over Africa. Analysis shows that the MME mainly captures the wide-scale spatial distribution of observed precipitation in CA with important rainfall in the CB in DJF and SON of ∼9.5 mm/day. However, a slight divergence is observable between the individual NMME and the MME.

The bias analysis shows a rather large bias of ∼5 mm/day in the MAM, DJF, and SON seasons for the CCSM3 and CCSM4 models. The CFSV1 and CFSV2 instead show a negative bias of ∼ −5 mm/day (see Figure 3d,f,g,h′) over all of Cameroon, Gabon, Congo, and a large part of the Central African Republic in the MAM, JJA and over the CB in the SON. The model CanCM3 shows a bias in the CB ∼ −5 mm/day in the DJF, MAM. However, it may be seen that slightly more than half of the models overestimate rainfall ∼3.5 to 4 mm/day over the Gulf of Guinea and the southwestern part of Cameroon near Mount Cameroon (see Figure 3). The MME overestimates DJF and MAM rainfall for the −5 to 5 N latitude band (Figure 3u′,v′) over CA. During all seasons in CA, it is clearly observed that the NMME models can simulate the distribution of climatology precipitation at lead 0, but the magnitude is relatively larger than the ARC2 observation for most models in the region.

During SON, the distribution of rainfall appears to be in reasonable concordance with the ARC2 over the entire study area. However, a wet bias exists and is observable in the majority of the NMME models. The results are compatible with those of Vizy et al. (2013) who identified a common wet bias over all of Africa in the Coupled Model Intercomparison Project 5 models and Tanessong et al. (2020) for the Climate-system Historical Forecast Project models over CA. In addition, using the Climate Hazards Group InfraRed Precipitation with Station dataset and Global precipitation Center (GPCC), Shukla et al. (2016) found a large bias of the NMME models greater than 4 mm/day over EA, also a similar bias of the MME about 5 mm/day over CA was identified by Tchinda et al. (2022) using GPCC and NMME CPC PRATE observation datasets. Some of the gap between the observation and models can be assigned to meridional large-scale temperature gradient and displacement of ITCZ in models (Richter & Xie, 2008), which may also cause a rainfall increase in the coastal areas of Equatorial Guinea and a decline in the north. The causes of these errors may also be related to failures in the physics of the model, such as failures in the modelling of global clouds and energy fluxes, with coarse-resolution climate models being inactive in simulating mesoscale convection (Acharya et al., 2011; Biasutti, 2013; Zebaze et al., 2019), which introduces biases in the global models.

3.2 | Model skill and errors

The TD and TSS are calculated for the NMME forecasts and MME in this sub-section. TD and TSS are calculated from 0 to 5 months lead time over the four seasons. SD and the PCC are determined relative to the reference observation (REF) ARC2. On the TD (see Figure 4), the colours red, blue, black, and green represent the DJF, MAM, JJA, and SON seasons, respectively. Each NMME model is represented by a number above the colour in the diagram. From 0 to 1 month lead time, the majority of NMME models over the four seasons generally agree better with the observation showing a PCC > 0.69 and TSS > 0.60. More than 90% of the models during DJF have a PCC > 0.90 and TSS > 0.80. The MME has a PCC of ∼0.96 and TSS of ∼0.85 for this same season. Overall, in the three seasons MAM, JJA, and SON, the TD shows a PCC in the 0.7 < PCC < 0.98 band. The IRI CHAM4P5, CFSV1 model, and MME have a slightly higher correlation ∼0.96 and TSS >0.82 at lead 1 in DJF, while the NCEP CFSV1 model in the MAM shows a high SD around 1.52 at lead 1. Note that SD > 1 indicates that simulated values are more variable than those of the observation used as reference (Sonkoué et al., 2019; Tamoffo et al., 2019; Tanessong et al., 2020). More than 98% of the NMME models in MAM (blue colour) have PCC between 0.2 < PCC <0.5, TSS < 0.65 and SD > 0.9 at lead 2 and lead 3. The seasons DJF, JJA, and SON in lead 2 show PCC between 0.50 < PCC < 0.90, and SD between 0.75 < SD < 1.53. The high values of correlations may be caused by a regular and more homogeneous climate in CA during these seasons. From 4 to 5 months lead time, most NMME forecasts indicate that PCC values decrease and attain a minimum of 0.12 with TSS fluctuations towards low values, but with a significant simulation of amplitude (i.e., SD). In addition, the NCEP CFSV2 model has the highest SD for the MAM compared with JJA and SON. The SD values for MAM of the latter model are ∼1.53 at lead 1, ∼1.51 at lead 0, ∼1.51 at lead 2, ∼1.53 at lead 3, ∼1.64 at lead 4, and ∼1.60 at lead 5. Over the three seasons, DJF, JJA, and SON at lead 5 about 85% of the NMME models are less correlated with a PCC <0.55 and can reach a minimum correlation value ∼0.1 for the models CanCM3, CCSM4, IRI CHAMP5, and MME in the seasons JJA (black colour on the TD) and DJF (red colour). In SON, still at lead 5 the models CCSM4, NCAR CESM1, CM2P5, and FLORAO6 have a TSS < 0.21 and the other models have

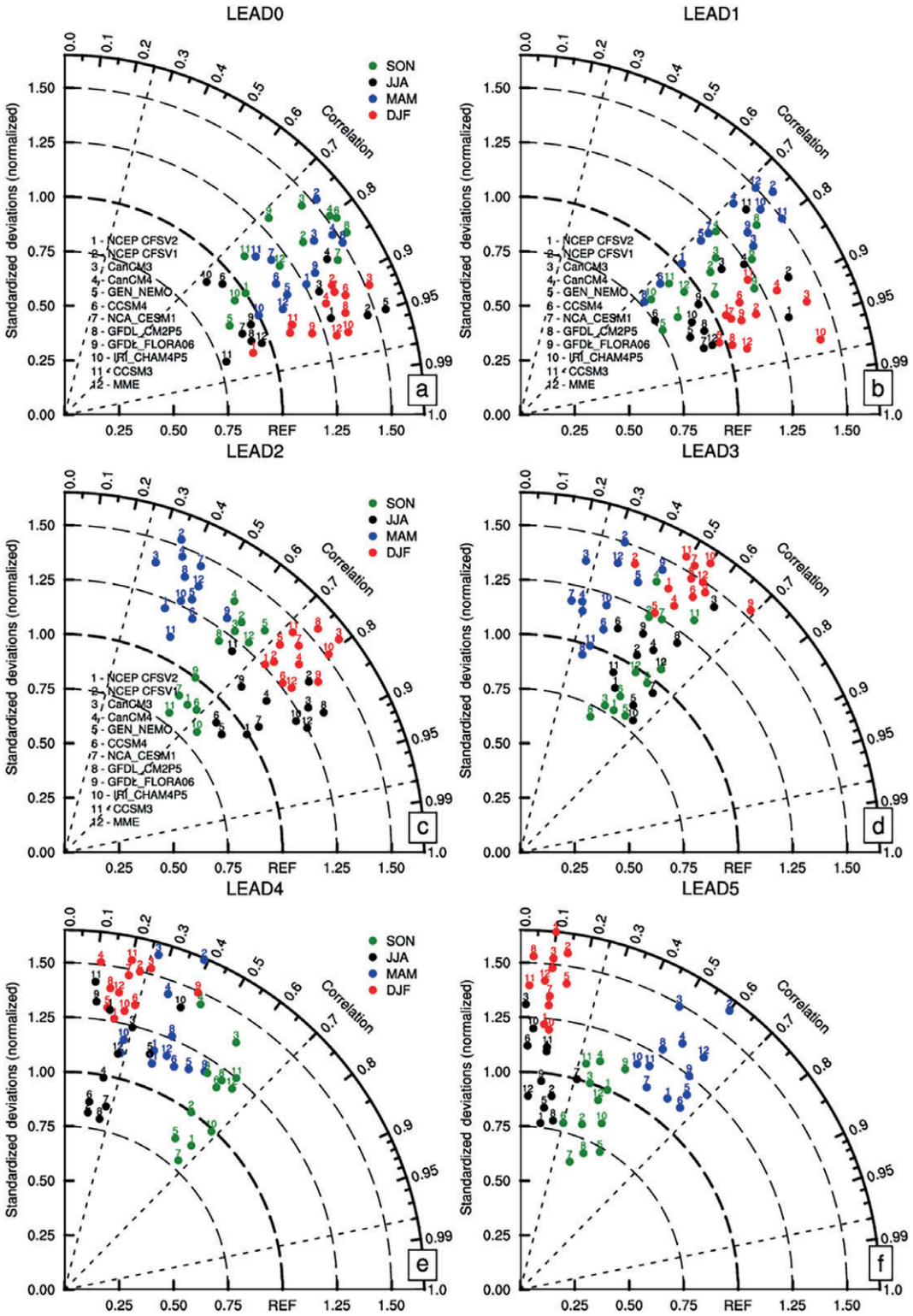

FIGURE 4 Taylor diagram between ARC2 reference observation and each individual North American Multi-Model Ensemble model (see Table 1) 0–5 months lead time over the four seasons December–February (DJF), March–May (MAM), June–August (JJA), and September–November (SON). Each season is represented by a colour in the diagram and each model is represented by a number above each colour.

TSS between 0.2 and 0.41. It follows that the relationship between the models and ARC2 as well as skill is relatively weak beyond the first lead time. The analysis of the scores shows that the NMME models skill is better for the first month of the forecast period. This result is justified by the chaotic dynamics of the atmosphere and the difficulties of climate models for long-term prediction (Kalnay, 2003), and also errors can come from the

initialization and parameterization of the model (Buizza et al., 2005; Schwierz et al., 2006). It is consistent with the results of the literature review, which indicate a good seasonal prediction of rainfall up to a few weeks or even a month in advance, with the predictive skill of the model being able to become approximately constant over time above 1–2 months (Crochemore et al., 2016). The assessment by season shows that the JJA and SON seem to be the best predicted by NMME models when bias and TSS are taken into account. This observation can be materialized by a more regular and uniform climate over CA during these different seasons. In addition, this corresponds to seasons where the rainfall accumulation is more comparable to the average. In general, the time scales have a high influence on the scores and quality of the seasonal forecasts in CA (Figure 5).

Given the low coverage of in situ data in CA, in addition to the ARC2 observation, we also evaluated the NMME models using the GPCC (A. Becker et al., 2013; Nicholson et al., 2003). The analyses show that over the four seasons, the NMME models reproduce reasonably well the spatial distribution of rainfall from the GPCC over the continent (see Figure S1), with a peak of rainfall ~10 mm/day observable over the Gulf of Guinea not far from Mount Cameroon in JJA. However, with this observation, the NMME models present an important bias in the region (Figure not shown) and require corrections before being used in domains such as hydrology. The TD between GPCC and NMME models (Figure S2) shows that the majority of the models have a PCC > 0.69 between 0 and 1 month lead time, which weakens as the lead time increases. Analysing the TSS between each individual model and the GPCC observation (Figure not shown), in DJF and SON, more than 70% of models have a TSS < 0.21 at lead 5.

The KGE from 0 to 5 months lead time of each NMME and MME is presented in Figure 6. The red, green, blue, and black collared curves represent the DJF, MAM, JJA, and SON seasons, respectively. The main results show that between lead 0 and lead 1 over 4 seasons about 85% of the models have positive KGE values between 0 and 0.4. The MME is ~0.4 at lead 0 and ~0.22 at lead 1. However, some NMME models at lead 0 have values higher than 0.5, namely the NCEP CFSV2 with KGE value of around 0.80 for the JJA and around 0.70 for the SON (black curve Figure 6a). The CanCM4 shows a value of ~0.51 for the JJA (blue curve Figure 6a). From 3 to 5 months lead time, several fluctuations in the KGE values are observable during the different seasons, and the predictive skill of the models becomes more limited. The NMME models show KGE values between $-0.4 < KGE < 0$ for MAM and JJA at lead 3. SON presents a relatively constant model performance in the range of 0–0.4 for 0–5 months lead time. At the lead 5, the MME has a KGE below −0.5 during DJF and JJA seasons (see Figure 6f).

3.3 | Categorical score: Heidke skill score and accuracy

In this section, we indicate that the accuracy by chance across three evenly likely categories is 0.33. Figures 7 and 8 show the HSS and accuracy for the four seasons of 0–5 months lead time between MME and ARC2, respectively; Figure S3 and Figure S4 show HSS and accuracy between MME and GPCC observation, respectively. Analysis of the HSS scores (see Figure 7 and Figure S3) shows values above 0 for the first three lead times in all seasons. The HSS shows a maximum of around 0.50 at lead 0 in the DJF and MAM, 0.70 and 0.54 in the JJA and SON, respectively (see Figure 7). HSS values are below 0 between 4 and 5 months lead time. Overall, the values of this score decrease like the metrics in the first part after the first three lead times and become negative thereafter at lead 4 and lead 5. The level of agreement between forecast and observation ARC2 (see Figure 8) and forecast and GPCC observation (Figure S4) illustrates that the accuracy is greater than 0.55 with ARC2 and greater than 0.50 with GPCC between 0 and 2 months lead time for all seasons. The highest values are observed at lead 0 for both observations used and reach a maximum value of 0.67 with the ARC2 and 0.61 with GPCC in JJA. The seasons DJF, MAM, and SON at lead 0 have accuracy values around 0.62, 0.64, and 0.60, respectively (see Figure 8). An accuracy of 0.67, 0.62, 0.64, and 0.60 means respectively that 67%, 62%, 64%, and 60% of MME rainfall forecast was correct. However, between 4 and 5 months lead time, the accuracy values are less than 0.45 using GPCC and ARC2 observations. Overall a decrease in accuracy is observed with increasing lead time. The results show that in CA, the performance of NMME models varies from season to season and from score to score. Moreover, the analyses show that lead time plays a major role in influencing the quality of seasonal forecasts. Similar to the previous analysis, HSS scores highlight that the performance decreases as the lead time increases. This may suggest that NMME models appear to have increasing constraints on maintaining a good quality seasonal forecast beyond several months (5 months) in the region.

Seasonal rainfall variability in CA is influenced by tropical ocean SST and this influence changes from season to season (Balas et al., 2007). These authors added that in much of the CA, seasonal rainfall variability is linked to pacific ENSO and the western Indian Ocean. In addition, Farnsworth et al. (2011) indicated that tropical SSTs are the main source of precipitation fluctuations

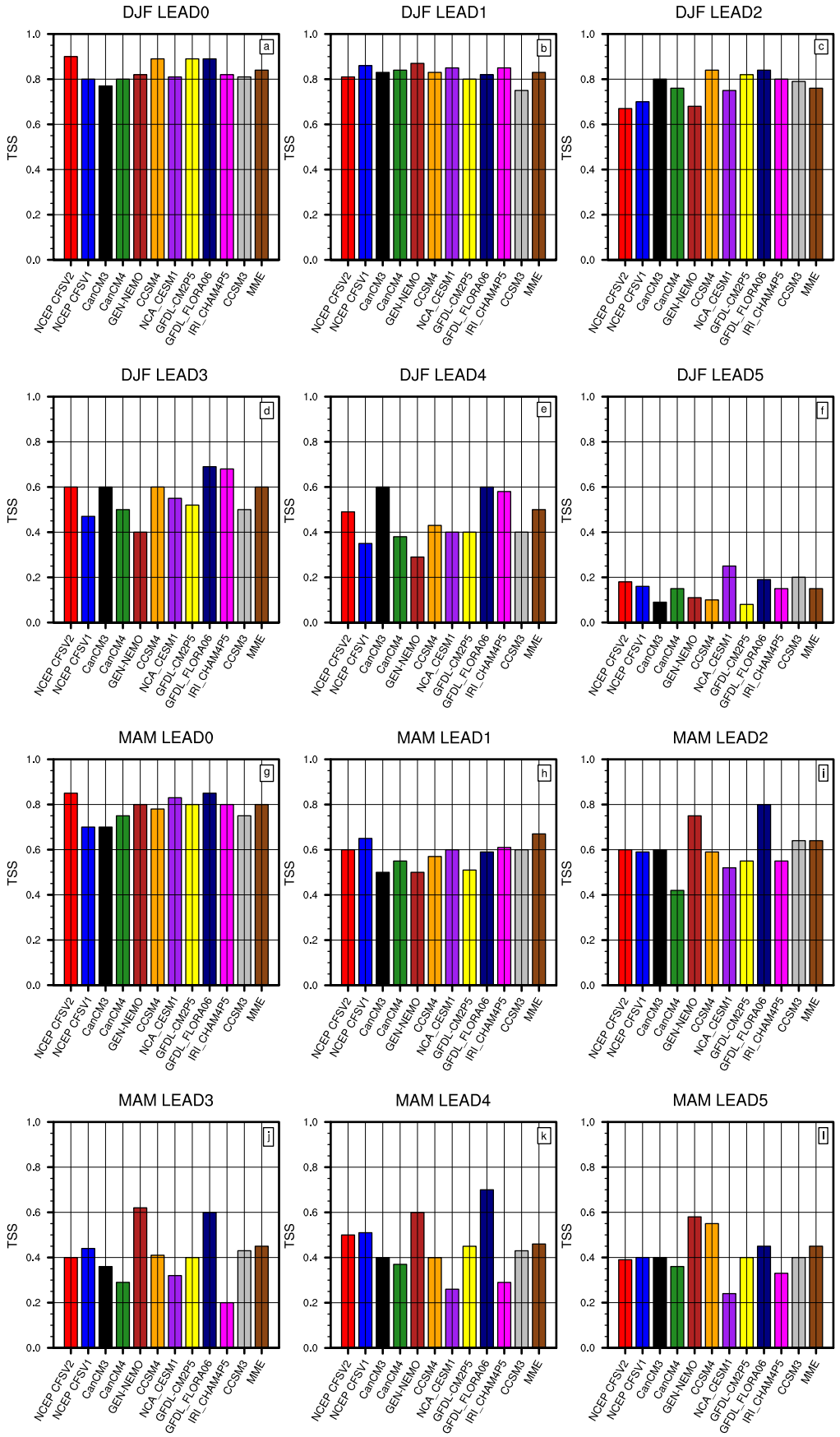

FIGURE 5 Taylor skill score (TSS) between the ARC2 observation and each individual North American Multi-Model Ensemble (NMME) for the different seasons from lead 0 to lead 5. a, b, c, d, e, f represents the December–February (DJF) and j, h, i, g, k, and l represents the March–May (MAM) season. TSS between the ARC2 observation and each individual NMME for the different seasons from lead 0 to lead 5. a′,b′,c′,d′,e′,f′ represents the June–August (JJA), and Figure 6j′,h′,i′,g′,k′,l′ represents the September–November (SON) season.

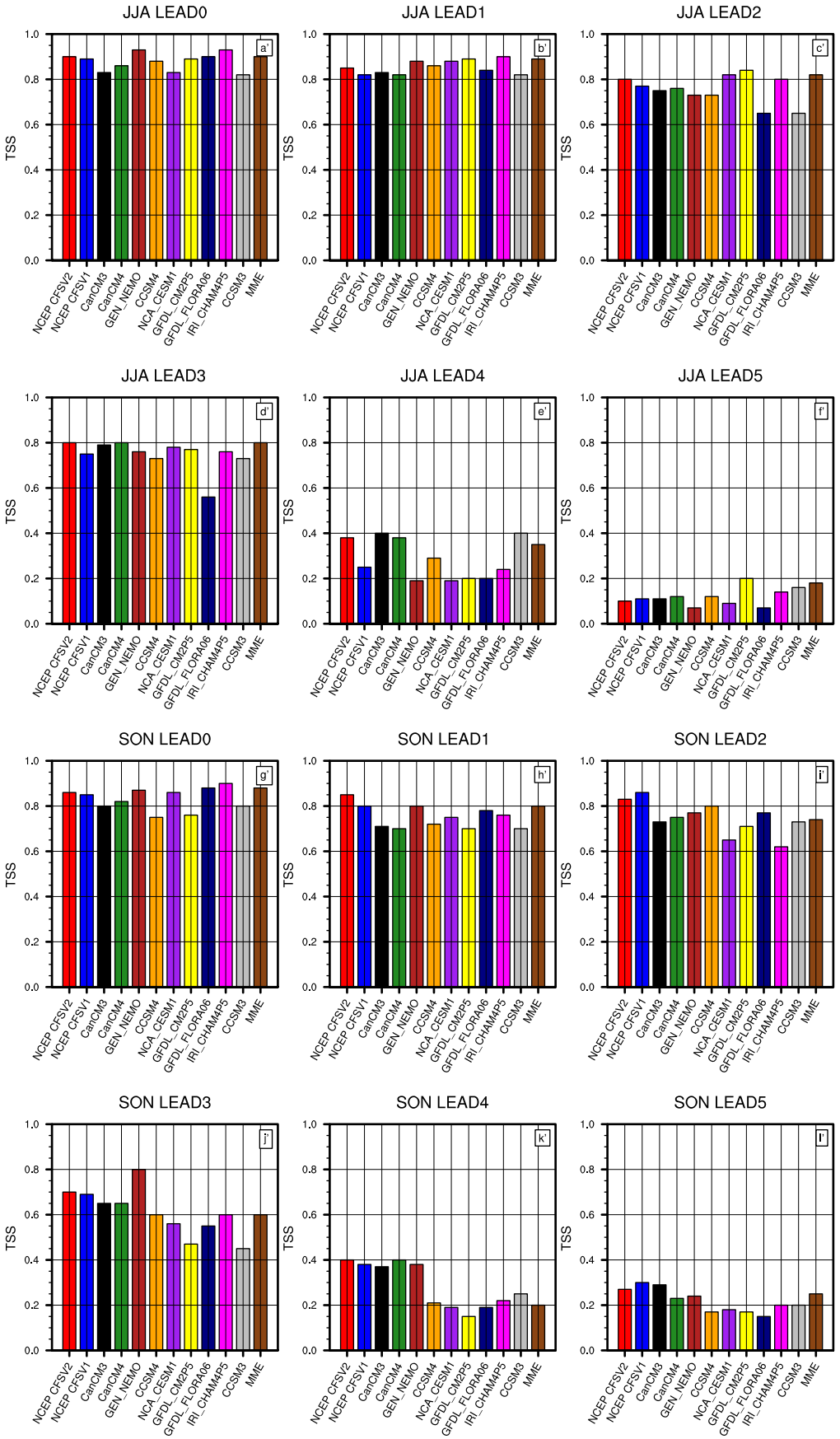

FIGURE 5 (Continued)

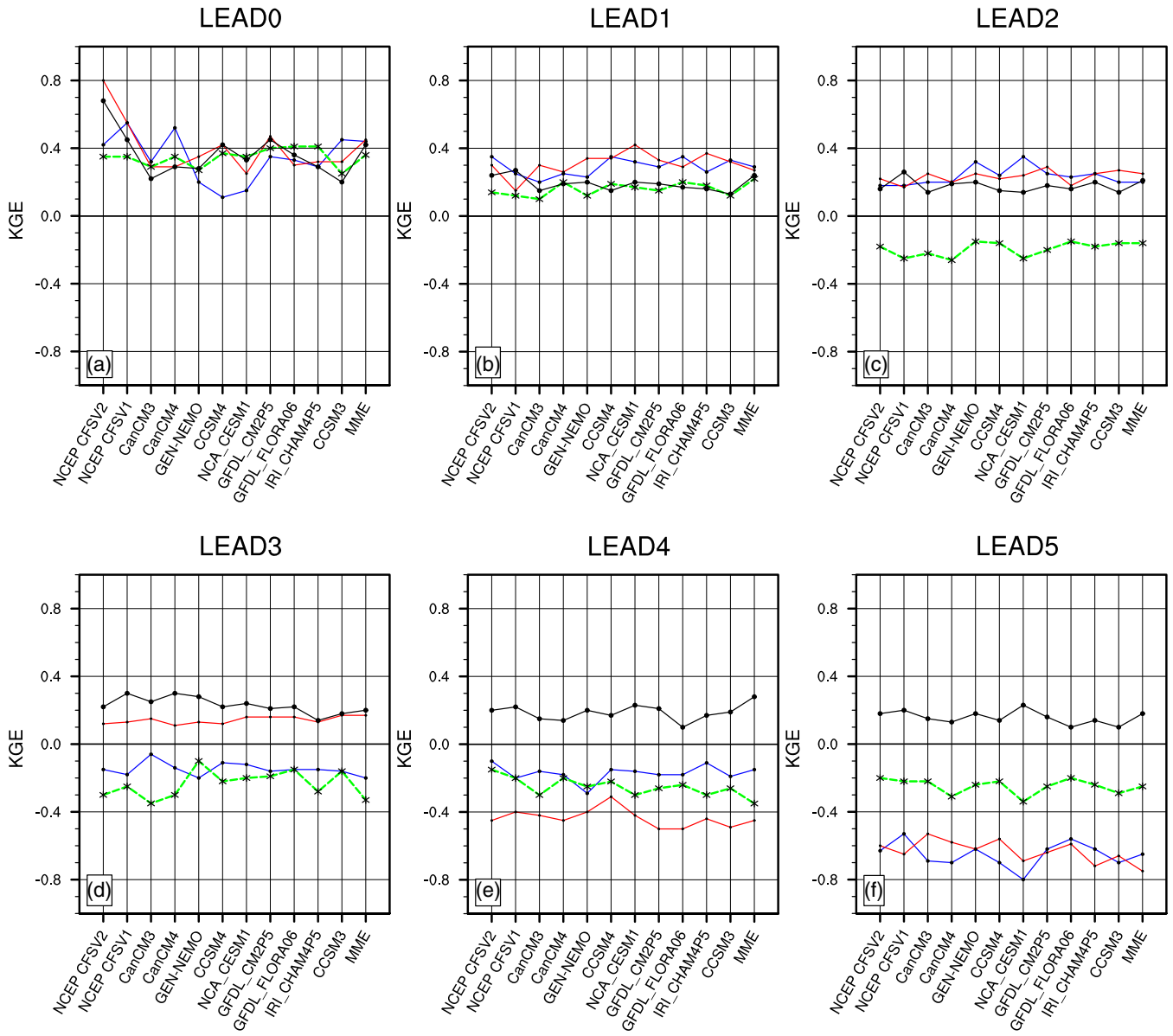

FIGURE 6 Diagram representing the Kling-Gupta efficiency (KGE) of each individual North American Multi-Model Ensemble (see Table 1) and NMME ensemble mean from 0 to 5 months lead time. The red, green, blue, and black curves in the diagram represent the December–February (DJF), March–May (MAM), June–August (JJA), and September–November (SON), respectively.

over CA. Given that, it is important in the remainder of this study to evaluate the skill of NMME models in reproducing SST anomalies over the western pole (IODWP), eastern pole (IODEP), and Niño 3.4 indices.

3.4 | Predictive skill of tropical SST

It is necessary to mention that seasonal forecasts using GCMs are of great concern due to the presence of systematic biases in the model simulation (Weisheimer et al., 2011). Thus, in addition to the chaotic dynamics of the atmosphere, which affect the seasonal predictability of the models, the tropical SST is the most important slowly varying boundary condition affecting tropical climate. The Pacific SST anomaly known as the ENSO and the Indian Ocean SST anomaly as IOD are the most important (Ashok et al., 2004; Pillai & Mohankumar, 2010; Rasmusson & Carpenter, 1983) with consequences that are being felt on a global scale.

As in Pillai et al. (2018), the skill of the different NMME for the SST index Niño 3.4 (5° S–5° N, 170°–120° W), SST anomalies over the western pole (IODWP) (10° S–10° N, 50°–70° E) and eastern pole (IODEP) (10° S–0°, 90°–110° E) are presented in Figures S5, S6, S7 respectively (see Supplementary Materials). In each of these figures, the abscissa axis represents the ACC between predicted and observed anomalies. The ordinate axis

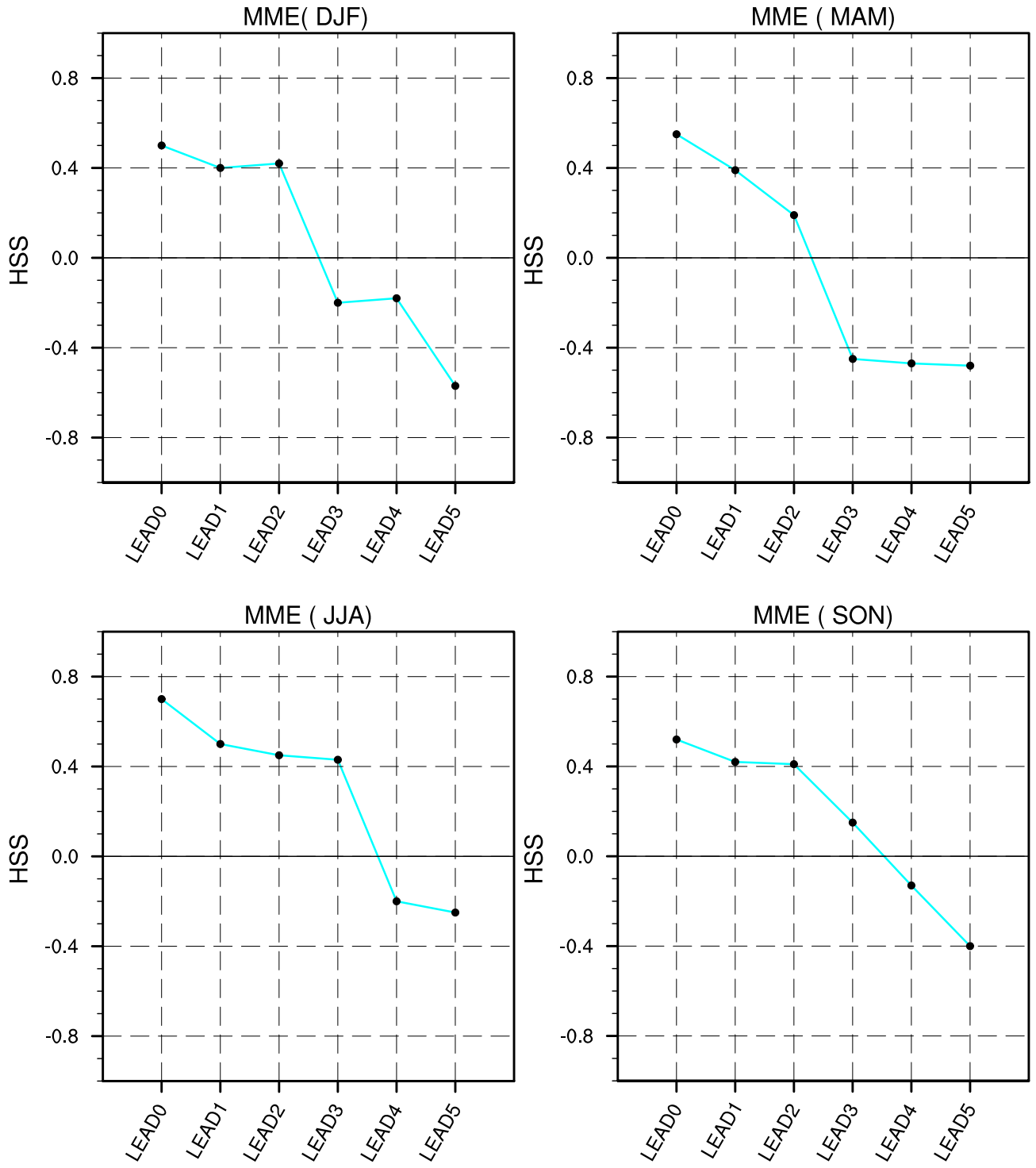

FIGURE 7 Diagram representing the Heidke skill score (HSS) over four seasons of the North American Multi-Model Ensemble ensemble mean (MME).

presents the ratio of SD on each of these figures. Columns 1, 2, 3, and 4 represent the DJF, MAM, JJA, and SON respectively, and rows 1–6 present lead 0 through lead 5 of each season. Thus, over the four seasons from lead 0 to lead 3, the index Niño3.4 present values of ACC > 0.55 for most of the NMME models except the model CanCM3 (ACC < 0.47) at lead 3 over all seasons, the model GFDL-FLOR A06 ($0.40 < \text{ACC} \leq 0.45$) at lead 2 over all seasons. However, between 4 and 5 months lead time over the four seasons, a slight decrease in the ACC is observed and the values are between 0.3 and 0.49. The model CanCM3 has the lowest value at lead 5 in the SON with an ACC ≤ 0.21. SD values increase slightly as lead time increases for most models. For the SST index

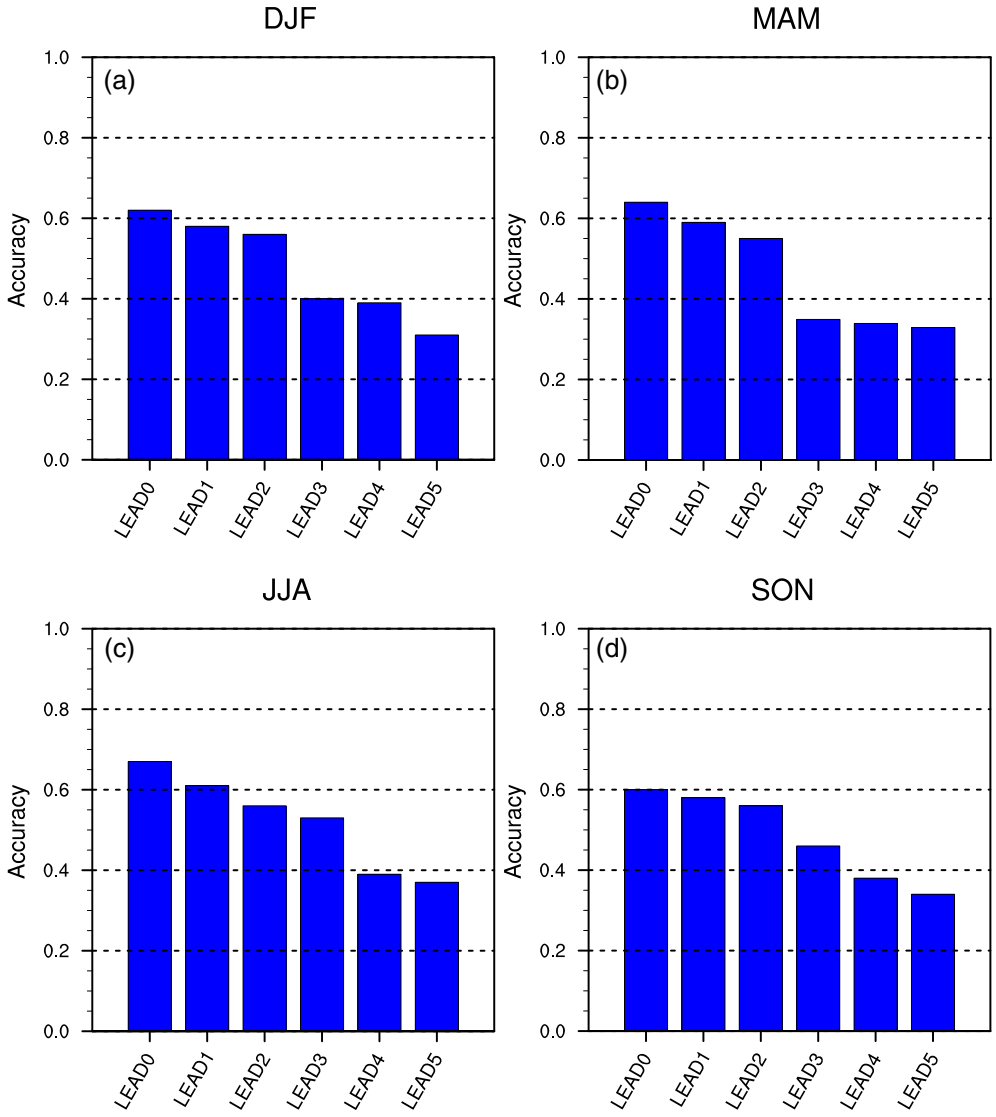

FIGURE 8 Accuracy between North American Multi-Model Ensemble ensemble mean and observation of the four seasons December–February (DJF), March–May (MAM), June–August (JJA), and September–November (SON) from lead 0 to lead 5.

IODEP (see Figure S6), most models have a low skill (ACC < 0.55), and SD < 1 including the MME over all seasons between 0 and 4 months lead time. Note that SD > 1 indicates that simulated values are more variable than those of the observation used as reference (Sonkoué et al., 2019). A few models such as IRI CHAM4P5, FLOR Ao6, CanCM4, GFDL CM2P5 show an exception by showing an ACC > 0.59 between lead 0 and lead 2. However, between lead 4 and lead 5, more than 80% of the models over all seasons have moderate skill 0.2 < ACC < 0.45, and amplitude (0.70 ≤ SD ≤ 0.90) over all seasons. By observing the SST index for the IODWP (see Figure S7), more than 90% of the models show higher model skill (ACC > 0.50) between lead 0 and lead 3 over all seasons. Despite some slight differences, the model skills are higher for the SST index IODWP compared with the IODEP between the first lead times, which may be related to the higher skill of El Niño and associated response of the western tropical Indian Ocean (Pillai et al., 2018). However, between 4 and 5 months lead time (Figure S7), a slight decrease in ACC is observed with values between 0.21 and 0.45 for most models and SD values between 0.70 and 0.97. The CFSV2 models and MME show better skill (ACC > 0.60 and SD < 0.70) over all seasons at lead 0 for SST index IODWP.

Although with some slight differences, our results are consistent with those of Pillai et al. (2018) who identified that the Niño 3.4 index had a skill (>0.5) for most NMME models and that the IODWP skills of NMME models were greater compared with IODEP. Recently, Moihamette et al. (2022) in CA found a strong correlation ($r = 0.63$) of the Niño 3.4 index during the SON season and mentioned that the IOD contributes to the variability of rainfall in CA towards the south, particularly in the East of the Democratic Republic of Congo, and over the area extending from Gabon to the Republic of Congo. Moreover, the skill of NMME models in predicting SST indices (ENSO, IOD) is very important for better prediction of rainfall simulations over land regions (Pillai et al., 2018). The high skill of SSTs at the first three lead times accompanies the model's high performance in

precipitation. Such a relationship is consistent with the notion that the tropical oceans (Atlantic, Pacific, and Indian) are the primary drivers of rainfall variability in Africa (Camberlin & Philippon, 2002; Preethi et al., 2015). In addition, the Indian Ocean has been identified as the primary source of ocean moisture for precipitation in CA (Dyer et al., 2017). Thus, the high performance of models simulating SSTs between 0 and 2 months lead time may suggest that ENSO, IODWP are good indicators to predict the increase or decrease of precipitation in the CA during this time interval. During extreme IOD events, CA receives high moisture from the Indian Ocean, which favours increased rainfall (Moihamette et al., 2022). This increase in rainfall may be one of the causes of some wet biases in NMME models observed in CA.

4 | SUMMARY AND CONCLUSION

The rainfall forecasts over Central Africa (CA), using the North American Multi-Model Ensemble (NMME) models, have been assessed over - hindcast period of 1983–2009 to guide model developers and users of seasonal forecasts of the region. The study was done for all seasons: December–February (DJF), March–May (MAM), June–August (JJA), and September–November (SON). The quality criteria chosen were: the climatology of each individual NMME and NMME ensemble mean (MME), the Taylor diagram, the Taylor skill score (TSS), the Kling-Gupta efficiency (KGE), accuracy, and Heidke skill score (HSS). Besides, from the results and discussions presented in Section 3, the following conclusions have been deduced:

1. 1The analysis of the climatology indicated that the NMME models largely capture the large-scale spatial distribution of observed rainfall in the region at lead 0 with maximum precipitation in JJA over the north and remarkable peaks for the NCEP CFSV1, NCEP CFSV2, CM2P5, CESM1 models around Mount Cameroon (southwest Cameroon). In addition, rainfall peaks of ∼8 mm/day over northern Cameroon and Eastern Central African Republic in JJA, ∼10 mm/day in SON, and DJF over Eastern Democratic Republic of Congo for MME are also observed.
2. 2The models show a large bias of ∼5 mm/day over the MAM, DJF, and SON seasons for the CCSM3 and CCSM4 models. The CFSV1 and CFSV2 show a bias of ∼ −5 mm/day overall in Cameroon, Gabon, Congo, and a large part of the Central African Republic in the MAM, JJA, and over the Congo Basin in the SON.
3. 3The models showed high pattern correlation coefficient (PCC) between 0 and 1 month lead times for all seasons. However, IRI CHAM4P5, CFSV1, and MME showed a higher correlation ∼0.96 and TSS >0.82 at lead 1 in DJF. Although there is a slight difference between 0 and 2 months lead time, it was found that between 4 and 5 months lead time, the models' performance decreases. Thus, at the lead 5 ∼85% of the models over the three seasons DJF, JJA, and SON are less correlated with a PCC < 0.55 and reach a minimum PCC value of ∼0.12 for the models CanCM3, CCSM4, IRI CHAMP5, and MME in JJA and DJF.
4. Seasonal forecasts over the four seasons resulting from the categorical analysis show that the accuracy between the NMME models and the observations is above the average (accuracy > 0.5) between 0 and 2 months lead time and less than 0.45 between 4 and 5 months lead time.
5. Despite a minor variation, the Niño3.4, IODWP, and IODEP teleconnections with the tropical SST are well represented by more than half of the NMME models for all seasons between 0 and 2 months lead time. It was observed that between 4 and 5 months lead time, there is a slight decrease in the skill of NMME models for Niño3.4, IODWP, and IODEP indices (ACC ≤ 0.45 for most models including MME) for all four seasons. The quality of the skill decreases slightly with increasing lead time. However, NMME models showed a greater skill for the SST index IODWP compared with IODEP between 0 and 1 month lead times.

The results of this study have direct implications for model users, policymakers, forecasters, and agencies that focus on this region such as the Regional Climate Outlook Forum for Central Africa coordinated by the African Centre of Meteorological Applications for Development. Although the NMME models are a promising tool for users of seasonal forecasts in this region, the skill of rainfall forecasts is limited beyond several months, and caution should be exercised in their use for decision-making purposes. Methods for de-biasing model parameters should be performed on raw model data. Additional analysis is required to provide an understanding of the physical basis of the NMME models capability in CA for better predictability.

AUTHOR CONTRIBUTIONS

Armand Feudjio Tchinda: Conceptualization (equal); data curation (equal); formal analysis (equal); funding acquisition (equal); investigation (equal); methodology (equal); resources (equal); software (equal); writing - original draft (equal); writing – review & editing (equal). **Roméo Stève Tanessong:** Formal analysis (equal); funding acquisition (equal); methodology (equal); resources (equal); validation (equal); visualization (equal). **Ossénatou Mamadou:**

Formal analysis (equal); investigation (equal); project administration (equal); resources (equal); validation (equal); visualization (equal). **Vanessa Tchida Diffo:** Funding acquisition (equal); methodology (equal); validation (equal). **Zephirin Djomou Yepdo:** Data curation (equal); software (equal); writing – review and editing (equal). **Jean Bio Chabi Orou:** Data curation (equal); methodology (equal); supervision (equal).

ACKNOWLEDGEMENTS

The first author would like to express sincere gratitude to the German Federal Ministry for Education through the German Academic Exchange Service (DAAD) for supporting this research. We thank the Editor Professor Dino Zardi, Associate Editor Lorenzo Giovannini, and the three anonymous reviewers for the time and helpful and constructive comments on our manuscript. We thank professor Maria Helena Ramos from IRSTEA, France for these multiple suggestions and orientations. We thank Dr Nonki Rodric Mérimé for his suggestions during the revision our manuscript. We also thank the "Institut de Mathématiques et de Sciences Physiques (IMSP)" and "Centre d'Excellence Africain en Science Mathématiques, Informatiques et Applications (CEA-SMIA)". We sincerely thank the modelling groups and research centres, namely (Center for Ocean-Land-Atmosphere Studies (COLA), University of Miami, Geophysical Fluid Dynamics Laboratory (GFDL), IRI, NASA, NCAR, and NCEP) for the creation, regular updating, and provision of their NMME models.

FUNDING INFORMATION

This work was supported by the German Academic Exchange Service (DAAD). In Region Scholarship Programme-IMSP Benin, no 57506853.

CONFLICT OF INTEREST

The authors have no conflicts of interest to declare for the content of this paper.

ORCID

Armand Feudjio Tchinda https://orcid.org/0000-0003-0517-9495

Roméo Stève Tanessong https://orcid.org/0000-0003-3804-5901

REFERENCES

Acharya, N., Kar, S.C., Kulkarni, M.A., Mohanty, U.C. & Sahoo, L. N. (2011) Multi-model ensemble schemes for predicting northeast monsoon rainfall over peninsular India. *Journal of Earth System Science*, 120(5), 795–805.

Acharya, N., Ehsan, M.A., Admasu, A., Teshome, A. & Hall, K.J.C. (2021) On the next generation (NextGen) seasonal prediction system to enhance climate services over Ethiopia. *Climate Services*, 24, 100272. https://doi.org/10.1016/j.cliser.2021.100272

Aloysius, N.R., Sheffield, J., Saiers, J.E., Li, H. & Wood, E.F. (2016) Evaluation of historical and future simulations of precipitation and temperature in Central Africa from CMIP5 climate models. *Journal of Geophysical Research-Atmospheres*, 121(1), 130–152.

Ashok, K., Chan, W.-L., Motoi, T. & Yamagata, T. (2004) Decadal variability of the Indian Ocean dipole. *Geophysical Research Letters*, 31, L24207. https://doi.org/10.1029/2004GL021345

Babaousmail, H., Hou, R., Ayugi, B., Ojara, M., Ngoma, H., Karim, R. et al. (2021) Evaluation of the performance of CMIP6 models in reproducing rainfall patterns over North Africa. *Atmosphere*, 12(4), 475.

Balas, N., Nicholson, S.E. & Klotter, D. (2007) The relationship of rainfall variability in west Central Africa to sea-surface temperature fluctuations. *International Journal of Climatology*, 27(10), 1335–1349.

Barnston, A.G. (1992) Correspondence among the correlation, RMSE, and Heidke forecast verification measures; refinement of the Heidke score. *Weather and Forecasting*, 7(4), 699–709.

Bauer, P., Thorpe, A. & Brunet, G. (2015) The quiet revolution of numerical weather prediction. *Nature*, 525(7567), 47–55.

Becker, A., Finger, P., Meyer-Christoffer, A., Rudolf, B., Schamm, K., Schneider, U. et al. (2013) A description of the global land-surface precipitation data products of the Global Precipitation Climatology Centre with sample applications including centennial (trend) analysis from 1901-present. *Earth System Science Data*, 5(1), 71–99.

Becker, E., Den dool, H.V. & Zhang, Q. (2014) Predictability and forecast skill in NMME. *Journal of Climate*, 27(15), 5891–5906.

Becker, E., Kirtmann, B.P. & Pegion, K. (2020) Evolution of the north American multi-model ensemble. *Geophysical Research Letters*, 47, e2020GL087408.

Biasutti, M. (2013) Forced Sahel rainfall trends in the CMIP5 archive. *Journal of Geophysical Research-Atmospheres*, 118(4), 1613–1623.

Biman, J.N., Tonye, J., Wandji, N., Nyambi, G. & Akoa, M. (2004) Factors affecting the technical efficiency among smallholder farmers in the slash and burn agriculture zone of Cameroon. *Food Policy*, 29(5), 531–545.

Buizza, R., Houtekamer, P., Pellerin, G., Toth, Z., Zhu, Y. & Wei, M. (2005) A comparison of the ECMWF, MSC, and NCEP global ensemble prediction systems. *Monthly Weather Review*, 133(5), 1076–1097.

Camberlin, P. & Philippon, N. (2002) The East African March–May rainy season: associated atmospheric dynamics and predictability over the 1968–97 period. *Journal of Climate*, 15, 1002–1019.

Cash, B.A., Manganello, J.V. & Kinter, J.L. (2019) Evaluation of NMME temperature and precipitation bias and forecast skill for South Asia. *Climate Dynamics*, 53(12), 7363–7380.

Chen, W., Jiang, Z. & Li, L. (2011) Probabilistic projections of climate change over China under the SRES A1B scenario using 28 AOGCMs. *Journal of Climate*, 24(17), 4741–4756.

Clover, J. (2003) Food security in sub-Saharan Africa: feature. *African Security Review*, 12, 5–15.

Crochemore, L., Ramos, M.H. & Pappenberger, F. (2016) Bias correcting precipitation forecasts to improve the skill of seasonal stream flow forecasts. *Hydrology and Earth System Sciences*, 20(9), 3601–3618.

Demargne, J., Wu, L., Regonda, S.K., Brown, J.D., Lee, H., He, M. et al. (2014) The science of NOAA's operational hydrologic ensemble forecast service. *Bulletin of the American Meteorological Society*, 95(1), 79–98.

Donner, L.J., Wyman, B.L., Hemler, R.S., Horowitz, L.W., Ming, Y., Zhao, M. et al. (2011) The dynamical core, physical parameterizations, and basic simulation characteristics of the atmospheric component AM3 of the GFDL global coupled model CM3. *Journal of Climate*, 24(13), 3484–3519.

Dyer, E.L., Jones, D.B., Nusbaumer, J., Li, H., Collins, O., Vettoretti, G. et al. (2017) Congo Basin precipitation: assessing seasonality, regional interactions, and sources of moisture. *Journal of Geophysical Research-Atmospheres*, 122(13), 6882–6898.

Ehsan, M.A., Tippett, M.K., Robertson, A.W., Almazroui, M., Ismail, M., Dinku, T. et al. (2021) Seasonal predictability of Ethiopian Kiremt rainfall and forecast skill of ECMWF's SEAS5 model. *Climate Dynamics*, 57, 1–17.

Farnsworth, A., White, E., Williams, C.J., Black, E. & Kniveton, D. R. (2011) Understanding the large scale driving mechanisms of rainfall variability over Central Africa. Advances in Global Change Research African Climate and Climate. *Change*, 101, 122. https://doi.org/10.1007/978-90-481-3842-5_5

Fotso-Nguemo, T.C., Vondou, D.A., Pokam, W.M., Djomou, Z.Y., Diallo, I., Haensler, A.T. et al. (2017) On the added value of the regional climate model REMO in the assessment of climate change signal over Central Africa. *Climate Dynamics*, 49(11), 3813–3838.

Giannini, A., Ali, A., Kelley, C.P., Lamptey, B.L., Minoungou, B. & Ndiaye, O. (2020) Advances in the lead time of Sahel rainfall prediction with the North American Multimodel Ensemble. *Geophysical Research Letters*, 47(9), e2020GL087341.

Gupta, H.V., Kling, H., Yilmaz, K.K. & Martinez, G.F. (2009) Decomposition of the mean squared error and NSE performance criteria: implications for improving hydrological modeling. *Journal of Hydrology*, 377(1–2), 80–91.

Hao, Z., Yuan, X., Xia, Y., Hao, F. & Singh, V.P. (2017) An overview of drought monitoring and prediction systems at regional and global scales. *Bulletin of the American Meteorological Society*, 98(9), 1879–1896.

Hillbrumer, C. & Moloney, G. (2012) When early warning is not enough lessons learned from the 2011 Somalia Famine. *Global Food Security*, 1, 20–28.

Jones, P.W. (1999) First-and second-order conservative remapping schemes for grids in spherical coordinates. *Monthly Weather Review*, 127(9), 2204–2210.

Kalnay, E. (2003) *Atmospheric modeling, data assimilation and predictability*. Cambridge, UK: Cambridge University Press.

Kirtman, B.P., Min, D., Infanti, J.M., Kinter, J.L., Paolino, D.A., Zhang, Q. et al. (2014) The North American multimodel ensemble: phase-1 seasonal-to-interannual prediction; phase-2 toward developing intraseasonal prediction. *Bulletin of the American Meteorological Society*, 95(4), 585–601.

Kling, H., Fuchs, M. & Paulin, M. (2012) Runoff conditions in the upper Danube basin under an ensemble of climate change scenarios. *Journal of Hydrology*, 424, 264–277.

Krakauer, N.Y. (2019) Temperature trends and prediction skill in NMME seasonal forecasts. *Climate Dynamics*, 53(12), 7201–7213. https://doi.org/10.1007/s00382-017-3657-2

Merryfield, W.J., Lee, W.S., Boer, G.J., Kharin, V.V., Scinocca, J.F., Flato, G.M. et al. (2013) The Canadian seasonal to interannual prediction system.Part I: models and initialization. *Monthly Weather Review*, 141(8), 2910–2945.

Moihamette, F., Pokam, W.M., Diallo, I. & Washington, R. (2022) Extreme Indian Ocean dipole and rainfall variability over Central Africa. *International Journal of Climatology*, 1-18. https://doi.org/10.1002/joc.7531

Molteni, F., Stockdale, T., Alonso-Balmaseda, M., Balsamo, G., Buizza, R., Ferranti, L. et al. (2011) The new ECMWF seasonal forecast system (system 4). ECMWF tech. Memo. pp. 49.

Ngoma, H., Wen, W., Ayugi, B., Babaousmail, H., Karim, R. & Ongoma, V. (2021) Evaluation of precipitation simulations in CMIP6 models over Uganda. *International Journal of Climatology*, 41(9), 4743–4768.

Nicholson, S.E. & Dezfuli, A.K. (2013) The relationship of rainfall variability in western equatorial Africa to the tropical oceans and atmospheric circulation. Part I: The boreal spring. *Journal of Climate*, 26(1), 45–65.

Nicholson, S.E., Some, B., Mccollum, J., Nelkin, E., Klotter, D., Berte, Y. et al. (2003) Validation of TRMM and other rainfall estimates with a high-density gauge dataset for West Africa. PartII: validation of TRMM rainfall products. *Journal of Applied Meteorology*, 42(10), 1355–1368.

Novella, N.S. & Thiaw, W.M. (2013) African rainfall climatology version 2 for famine early warning systems. *Journal of Applied Meteorology and Climatology*, 52(3), 588–606.

Ogallo, L. & Oludhe, C. (2009) Climate information in decision-making in the Greater horn of Africa: lessons and experiences. *World Meteorological Organization (WMO) Bulletin*, 58, 184.

Pillai, P.A. & Mohankumar, K. (2010) Individual and combined influence of El Nino–Southern oscillation and Indian Ocean dipole on the tropospheric biennial oscillation. *Quarterly Journal of the Royal Meteorological Society*, 136(647), 297–304.

Pillai, P.A., Rao, S.A., Ramu, D.A., Pradhan, M. & George, G. (2018) Seasonal prediction skill of Indian summer monsoon rainfall in NMME models and monsoon mission CFSv2. *International Journal of Climatology*, 38, e847–e861.

Preethi, B., Sabin, T.P., Adedoyin, J.A. & Ashok, K. (2015) Impacts of the ENSO Modoki and other tropical Indo-Pacific climate-drivers on African rainfall. *Scientific Reports*, 5(1), 1–14. https://doi.org/10.1038/srep16653

Pu, B. & Cook, K.H. (2010) Dynamics of the West African westerly jet. *Journal of Climate*, 23(23), 6263–6276.

Rasmusson, E.M. & Carpenter, T.H. (1983) The relationship between eastern equatorial pacific sea surface temperatures and rainfall over India and Sri Lanka. *Monthly Weather Review*, 111, 517–528.

Reynolds, R.W., Rayner, N.A., Smith, T.M., Stokes, D.C. & Wang, W. (2002) An improved in situ and satellite SST analysis for climate. *Journal of Climate*, 15, 1609–1625.

Richter, I. & Xie, S.-P. (2008) On the origin of equatorial Atlantic biases in coupled general circulation models. *Climate Dynamics*, 31(5), 587–598.

Roy, T., He, X., Lin, P., Beck, H.E., Castro, C. & Wood, E.F. (2020) Global evaluation of seasonal precipitation and temperature forecasts from NMME. *Journal of Hydrometeorology*, 21(11), 2473–2486.

Saha, S., Moorthi, S., Wu, X., Wang, J., Nadiga, S., Tripp, P. et al. (2014) The NCEP climate forecast system version 2. *Journal of Climate*, 27(6), 2185–2208.

Schwierz, C., Appenzeller, C., Davies, H.C., Liniger, M.A., Müller, W., Stocker, T.F. et al. (2006) Challenges posed by and approaches to the study of seasonal-to-decadal climate variability. *Climatic Change*, 79(1–2), 31–63.

Setiawan, A.M., Koesmaryono, Y., Faqih, A. & Gunawan, D. (2017) North American multi model ensemble (NMME) performance of monthly precipitation forecast over south Sulawesi, Indonesia. *IOP Conference Series: Earth and Environmental Science*, 58(1), 012035.

Shukla, S., Roberts, J., Hoell, A., Funk, C.C., Robertson, F. & Kirtman, B. (2016) Assessing North American multimodel ensemble (NMME) seasonal forecast skill to assist in the early warning of anomalous hydrometeorological events over East Africa. *Climate Dynamics*, 53(12), 7411–7742.

Simon, M.H., Ziegler, M., Bosmans, J., Barker, S., Reason, C.J.C. & Hall, I.R. (2015) Eastern South African hydroclimate over the past 270,000 years. *Scientific Reports*, 5(1), 1–10.

Singh, B., Cash, B., Kinter, I.I.I. & James, L. (2019) Indian summer monsoon variability forecasts in the North American multi-model ensemble. *Climate Dynamics*, 53(12), 7321–7334.

Slater, L.J., Villarini, G. & Bradley, A.A. (2019) Evaluation of the skill of North-American Multi-Model Ensemble (NMME) global climate models in predicting average and extreme precipitation and temperature over the continental USA. *Climate Dynamics*, 53(12), 7381–7396. https://doi.org/10.1007/s00382-016-3286-1

Sonkoué, D., Monkam, D., Fotso-Nguemo, T.C., Yepdo, Z.D. & Vondou, D.,.A. (2019) Evaluation and projected changes in daily rainfall characteristics over Central Africa based on a multi model ensemble mean of CMIP5 simulations. *Theoretical and Applied Climatology*, 137(3), 2161–2186.

Stankis, H.R., Wilson, L.J. & Burrows, W.R. (1989) *Survey of common verification methods in meteorology*. Geneva: World Meteorological Organization.

Sylla, M.B., Coppola, E.M., Giorgi, L., Ruti, F., Dell' Aquila, P.M. & Bi, A. (2010) Multiyear simulation of the African climate using a regional climate model (RegCM3) with the high-resolution ERA-interim reanalysis. *Climate Dynamics*, 35(1), 231–247.

Tamoffo, A.T., Moufouma-Okia, W., Dosio, A., James, R., Pokam, W.M., Vondou, D.A. et al. (2019) Process-oriented assessment of RCA4 regional climate model projections over the Congo Basin under 1.5 c and 2 c global warming levels: influence of regional moisture fluxes. *Climate Dynamics*, 53(3), 1911–1935.

Tanessong, R.S., Fotso-Nguemo, T.C., Mbienda, A.J., Guenang, G. M., Sandjon, A.T., Kaissassou, S. et al. (2020) Assessing Climate-system Historical Forecast Project (CHFP) seasonal forecast skill over Central Africa. *Theoretical and Applied Climatology*, 140, 1515–1526.

Taylor, K.E. (2001) Summarizing multiple aspects of model performance in a single diagram. *Journal of Geophysical Research-Atmospheres*, 106(D7), 7183–7192.

Tchinda, A.F., Tanessong, R.S., Mamadou, O. & Orou, J.B.C. (2022) Assessing precipitation seasonal forecasts in Central Africa using North American Multimodel Ensemble (NMME). *Theoretical and Applied Climatology*, 147, 1–17. https://doi.org/10.1007/s00704-021-03915-3

Teshome, A., Zhang, J., Ma, Q., Zebiak, S.E., Demissie, T., Dinku, T. et al. (2022) Skill assessment of North American Multi-Models Ensemble (NMME) for June-September (JJAS) seasonal rainfall over Ethiopia. *Atmospheric and Climate Sciences*, 12, 54–73. https://doi.org/10.4236/acs.2022.121005

Thober, S., Kumar, R., Sheffield, J., Mai, J., Schafer, D. & Samaniego, L. (2015) Seasonal soil moisture drought prediction over Europe using the North American Multi-Model Ensemble (NMME). *Journal of Hydrometeorology*, 16(6), 2329–2344.

Tierney, J.E., Smerdon, J.E., Anchukaitis, K.J. & Seager, R. (2013) Multidecadal variability in East African hydroclimate controlled by the Indian Ocean. *Nature*, 493(7432), 389–392.

Tippett, M.K., Barnston, A.G. & Robertson, A.W. (2007) Estimation of seasonal precipitation tercile-based categorical probabilities from ensembles. *Journal of Climate*, 20(10), 2210–2228.

Vizy, E.K., Cook, K.H., Crétat, J. & Neupane, N. (2013) Projections of a wetter Sahel in the twenty-first century from global and regional models. *Journal of Climate*, 26(13), 4664–4687.

Wang, H. (2014) Evaluation of monthly precipitation forecasting skill of the National Multi-model Ensemble in the summer season. *Hydrological Processes*, 28(15), 4472–4486.

Wang, B., Zheng, L.D., Liu, L., Ji, F., Clark, A. & Yu, Q. (2018) Using multi-model ensembles of CMIP5 global climate models to reproduce observed monthly rainfall and temperature with machine learning methods in Australia. *International Journal of Climatology*, 38(13), 4891–4902.

Washington, R.J., Rachel, P., Pokam, W.M. & Moufouma-Okia, W. (2013) Congo Basin rainfall climatology: can we believe the climate models? *Philosophical Transactions of the Royal Society, B: Biological Sciences*, 368(1625), 20120296.

Weisheimer, A., Palmer, T. N. & Doblas-Reyes, F. J. (2011) Assessment of representations of model uncertainty in monthly and seasonal forecast ensembles. *Geophysical Research Letters*, 38, L16703. doi:10.1029/2011GL048123.

Yao, M.N. & Yuan, X. (2018) Evaluation of summer drought ensemble prediction over the Yellow River basin. *Atmospheric and Oceanic Science Letters*, 11(4), 314–321.

Yuan, X., Roundy, J.K., Wood, E.F. & Sheffield, J. (2015) Seasonal forecasting of global hydrologic extremes: system development and evaluation over GEWEX basins. *Bulletin of the American Meteorological Society*, 96(11), 1895–1912.

Zebaze, S., Jain, S., Salunke, P., Shafiq, S. & Mishra, S.K. (2019) Assessment of CMIP5 multimodel mean for the historical climate of Africa. *Atmospheric Science Letters*, 20(8), e926.

Zhao, T., Zhang, Y. & Chen, X. (2018) Predictive performance of NMME seasonal forecasts of global precipitation: a spatial-temporal perspective. *Journal of Hydrology*, 570, 17–25.

Zhou, Y. & Kim, H.-M. (2018) Prediction of atmospheric rivers over the North Pacific and its connection to ENSO in the North American multi-model ensemble (NMME). *Climate Dynamics*, 51(5), 1623–1637.

Zhu, H., Jiang, Z., Li, J., Li, W., Sun, C. & Li, L. (2020) Does CMIP6 inspire more confidence in simulating climate extremes over China? *Advances in Atmospheric Sciences*, 37(10), 1119–1132.

SUPPORTING INFORMATION

Additional supporting information may be found in the online version of the article at the publisher's website.

How to cite this article: Feudjio Tchinda, A., Tanessong, R. S., Mamadou, O., Tchida Diffo, V., Djomou Yepdo, Z., & Chabi Orou, J. B. (2022). Predictive skill of North American Multi-Model Ensemble seasonal forecasts for the climate rainfall over Central Africa. *Meteorological Applications*, *29*(3), e2074. https://doi.org/10.1002/met.2074